





## Article

# Reliability Enhancement of Photovoltaic Systems under Partial Shading through a Two-Step Module Placement Approach

Belqasem Aljafari <sup>1</sup>, Priya Ranjan Satpathy <sup>2</sup>, Siva Rama Krishna Madeti <sup>3</sup>, Pradeep Vishnuram <sup>4,\*</sup>  
and Sudhakar Babu Thanikanti <sup>2,\*</sup>

<sup>1</sup> Department of Electrical Engineering, College of Engineering, Najran University, Najran 11001, Saudi Arabia

<sup>2</sup> Department of Electrical and Electronics Engineering, Chaitanya Bharathi Institute of Technology, Hyderabad 500075, India

<sup>3</sup> Department of Electrical and Electronics Engineering, SRKR Engineering College, Bhimavaram 534204, India

<sup>4</sup> Department of Electrical and Electronics Engineering, SRM Institute of Science and Technology, Chennai 603203, India

\* Correspondence: pradeep.kannan03@gmail.com (P.V.); sudhakarbabu@ieee.org (S.B.T.)

**Abstract:** Partial shading has a negative impact on photovoltaic systems by forcing the connected modules to generate lower power, creating severe unexpected power losses. To resolve this issue, numerous solutions have been proposed, among which configuration modification has recently attracted a greater audience. The preliminary approach to module reconfiguration was based on the alteration of electrical connections through switches, which introduces lag due to the large number of switches and sensors, complex algorithms, and impractical application. Hence, static techniques are considered to be a cost-effective, low-complexity and easy-to-adopt solution for efficiently reducing the losses due to shading. Hence, this paper proposes a two-step module replacement approach that is validated under multiple partial shading conditions, and the performance is compared with various conventional and hybrid configurations and a static electrical reconfiguration technique using mathematical analysis, comparative parameters and power curves analysis. The validation was performed using the MATLAB platform for two system sizes— $6 \times 6$  and  $18 \times 3$ —proving its applicability for arbitrary system sizes. On the basis of the depth investigation, an average power increase of 17.49%, 14.47%, and 14.12% for the two-step approach compared to the conventional, hybrid and electrical reconfiguration was observed in the partial shading cases considered.

**Keywords:** efficiency; maximum power point; partial shading; power loss; reconfiguration; solar photovoltaic



**Citation:** Aljafari, B.; Satpathy, P.R.; Madeti, S.R.K.; Vishnuram, P.; Thanikanti, S.B. Reliability Enhancement of Photovoltaic Systems under Partial Shading through a Two-Step Module Placement Approach. *Energies* **2022**, *15*, 7766. <https://doi.org/10.3390/en15207766>

Academic Editors: Jesús Manuel Riquelme-Santos and Adel Mellit

Received: 28 September 2022

Accepted: 17 October 2022

Published: 20 October 2022

**Publisher's Note:** MDPI stays neutral with regard to jurisdictional claims in published maps and institutional affiliations.



**Copyright:** © 2022 by the authors. Licensee MDPI, Basel, Switzerland. This article is an open access article distributed under the terms and conditions of the Creative Commons Attribution (CC BY) license (<https://creativecommons.org/licenses/by/4.0/>).

## 1. Introduction

Solar Photovoltaic (PV) systems have emerged as a viable source among all renewables due to their lower degree of required maintenance, location-independent installation, costless generation, and ease of implementation [1]. Additionally, recent advances in terms of efficiency and cost reduction in PV technologies have prompted installers to opt for solar PV systems [2]. In recent years, the governments of many developing countries have taken various initiatives by providing incentives and tax relief for solar PV system installation in order to reduce their nations' energy dependence on fossil fuels [3]. Hence, PV systems are turning out to be the most reliable and a major source of energy generation for industrial, residential and office sectors, facilitating a reduction in electricity consumption from the grid, and hence a reduction in environmental impact [4].

PV systems are expected to generate the maximum power throughout their operational period; however, various unavoidable phenomena affect system performance and raise reliability questions [5]. One of the main factors reducing the performance of the system is partial shading among the modules occurring due to natural phenomena such as shadows caused by nearby objects, clouds, dust, etc., creating multiple irradiance operation scenarios

for connected modules [6]. In this case, each of the modules generates power based on their respectively received irradiances, creating an operation mismatch in the system, resulting in lower power output and increased complexity [7]. Additionally, additional complexities occur when the bypass diodes of the modules get turned on and result in distortion of the characteristics curves by exhibiting multiple peaks, causing power loss in the maximum power tracking level of the DC converter [8]. These complexities can be solved through the implementation of modified maximum power point tracking (MPPT) algorithms based on various optimization techniques that have the capability of tracking the actual maximum power point from distorted curves [9]. Some recently proposed modified MPPT algorithms are based on the Neighboring Pixel technique [10], Nelder–Mead simplex technique [11], hybrid GWO–PSO technique [12], Social Grouping technique [13], and many more [14]. These algorithms have higher tracking speed, along with an efficiency of more than 90%; however, practical implementation, cost, algorithm complexities and adaptability to shading are the major constraints affecting the reliability of these techniques. Similarly, various power electronics solutions based on DC–DC converter architectures known as differential power processors (DPP) have recently been proposed to mitigate the system losses caused by partial shading [15]. Based on these DPP architectures, a TCT-SC system has been proposed and implemented for arbitrary array sizes, and the conversion efficiency was found to be 97% [16]. Similarly, a module-to-panel modular converter has been proposed in which the PV system contains an isolated DC bus and the experimental validation showed that the system had a 5.6% higher annual energy yield during partial shading [17]. Additionally, another switched capacitor-based DPP for a large PV power plant was proposed, and the field testing showed an average energy yield of 10–20% in the system during partial shading [18]. These converters are highly reliable and efficient for the mitigation of partial shading in PV arrays; however, major limitations arise with respect to the requirement of individual design for arbitrary sizes, cost, and high-power applications. Hence, considering the above limitations of these shading mitigation techniques, recently, most research has been focused on array configurations with the aim of reducing losses in the system with the advantages of low cost, lower complexity, higher reliability, and ease of implementation.

Previously proposed cost-effective solutions include array configurations constructed by applying additional wires between the connecting junctions of modules to facilitate the flow of electrical currents. The commonly used and conventional categories include: series-parallel, bridge-linked, honeycomb and total-cross-tied, denoted as SP, BL, HC and TCT, respectively [19]. Most simulation and experimental analyses show the higher effectiveness of TCT [20], whereas some studies show that configurations have the least effect under shading caused by clouds [21]. Subsequently, considering the redundancy and complexities of the wires, various configurations based on hybridization of the conventional configurations were proposed, tested, and proved to be more efficient than SP, BL and HC [22]. Further modification resulted in the introduction of array reconfiguration, a configuration performed under two mechanisms, i.e., dynamic electrical reconnection or static relocation of modules connected to the array with the main aim of dispersing the shading effect throughout the array to reduce current differences between rows [23]. Dynamic reconfiguration strategies implement optimization techniques to change the electrical connection of the TCT-connected modules through a switching matrix that gives the optimal connection between modules by calculating the minimum current difference between rows [24]. Recently, a dynamic reconfiguration based on the dragonfly optimization algorithm was proposed, and was found to have 22%, 10%, 2.95% and 1.07% higher power than static, dynamic and EAR, respectively [25]. Another fully dynamic neuro-fuzzy algorithm reconfiguration was proposed and validated experimentally and concluded to have 10% higher power than conventional systems [26]. Another African vulture optimization approach was proposed and compared with total cross-tied (TCT), Sudoku, Harris Hawks optimizer (HHO), Aquila optimizer (AO), and antlion optimizer (ALO), and was found to present higher power enhancement and a performance ratio of 39.91% and 82.91%, respectively [27].

Reconfiguration based on the Follow The Regularized Leader (FTRL) prediction model showed better performance than other dynamic reconfigurations under all the shading scenarios, offering better shade ability [28]. Similarly, another reconfiguration based on the genetic algorithm optimization technique was proposed, and it was found that the GA-based tool was able to work under changing environmental conditions and generate higher power output under all shading cases [29]. The algorithms proposed above have the advantage of higher power output during partial shading than conventional configurations; however, the major demerits include requiring large sensors and switches, complex algorithms for the switching matrix, and real-time application, as none of these algorithms have been tested experimentally. Hence, in contrast, static reconfigurations are gaining importance due to their not requiring switches or sensors, and there being no dynamic sections, as well as their ability to generate higher power than conventional techniques. The static reconfiguration begins with the proposal of a fixed electrical connection that has been validated experimentally using a  $5 \times 5$  array and found to have a higher performance than conventional techniques [30]. Another well-known reconfiguration technique is the Sudoku technique, where the modules of the array are physically relocated to disperse the shading and validated using a  $9 \times 9$  array [31]. A zig-zag reconfiguration was proposed and compared with conventional TCT, OTCT and NTCT schemes and found to have a higher power output [31]. Another novel magic square-based reconfiguration technique for PV arrays was proposed and compared with TCT, and it was found to offer a power enhancement of 11.53% under partial shading [32]. Another magic square algorithm was proposed and found to have higher power output than the Sudoku or Optimal-Sudoku, offering higher power output with reduced losses during shading [33]. Most recently, a four-square Sudoku reconfiguration was proposed and evaluated in comparison with several static and dynamic reconfiguration approaches, and was found to have 38.016% higher power [34]. An Ancient Chinese Magic square reconfiguration was proposed, compared with TCT and Sudoku, and concluded to offer higher power output during partial shading on the basis of simulation and experimental validations [35]. An improved non-symmetrical reconfiguration puzzle reconfiguration scheme was proposed that introduced an odd–even configuration and redefined the shift distance in order to obtain a static reconfiguration [36]. A new skyscraper puzzle-based one-time reconfiguration has been proposed, tested using  $5 \times 5$  and  $9 \times 9$  arrays, compared with TCT, Dominance Square and Sudoku technique, and found to have higher shade dispersion capability during partial shading [37]. A ken-ken puzzle pattern-based reconfiguration was proposed, tested in a  $4 \times 4$  array and found to offer a 10.85% power improvement compared to LS, Sudoku, and OE [38]. However, these techniques are typically validated using symmetric arrays such as  $9 \times 9$  which are not common in real-world scenarios, and their application to asymmetric arrays has not been investigated. A one-time electrical reconfiguration was proposed for PV arrays and was found to have 20% higher power output than the conventional PV array configurations [39]. However, the technique has been compared with limited configurations and the performance with respect to other techniques has not been studied. Recently, a digital image encryption-based reconfiguration was proposed and tested using  $9 \times 9$ ,  $7 \times 7$ ,  $6 \times 6$ ,  $5 \times 5$ ,  $4 \times 4$ ,  $3 \times 5$ ,  $4 \times 3$ ,  $5 \times 9$ , and  $6 \times 20$  array sizes and compared with 41 reconfiguration techniques under 100 distinct shading cases [40]. The proposed technique exhibited 30.81%, 36.36%, 38.15%, 33.77%, 16.62%, 21.8%, 18.42%, and 16.79% higher power output in the  $9 \times 9$ ,  $7 \times 7$ ,  $6 \times 6$ ,  $5 \times 5$ ,  $4 \times 4$ ,  $4 \times 3$ ,  $5 \times 9$ , and  $6 \times 20$  PV arrays, respectively. However, the algorithm proposed in that work was based on image encryption, which is complex and needs proper understanding related to the image encryption methodology. Another 64 various reconfigurations have been reviewed in the literature, where it is stated that most static reconfiguration techniques are limited to symmetric arrays and are difficult to implement in practical scenarios [41,42]. Additionally, it is stated that dynamic reconfigurations are costly due to the requirement of switches, sensors and control algorithms, which increase the cost of the system.

Hence, in this paper, a two-step approach based on the combination of two-times position replacement of modules is proposed, which is applicable for both symmetric and asymmetric arrays and enhances the reliability of the arrays during partial shading. The proposed technique is static, in that it contains no dynamic parts, switches, sensors, or complex algorithms, and can be effectively implemented in arbitrary array sizes with no additional complexity. The validation of the proposed technique is performed using two array sizes of  $6 \times 6$  (short) and  $18 \times 3$  (long) in the MATLAB/Simulink platform under numerous shading patterns. The power–voltage curves, maximum power output, mismatch loss, power reduction, power increment, efficiency, and performance index of the proposed approach are compared to that of conventional SP, BL, HC and TCT configurations, hybrid SP-TCT, BL-TCT, HC-TCT and BL-HC, and static electrical reconfiguration methodology under shading cases.

The remainder of this paper provides a description of the mathematical modeling of the PV modules and formulations in Section 2, a description of conventional and hybrid configurations in Section 3, an explanation of the implementation of the proposed two-step approach for the arrays in Section 4, an analysis under numerous partial shading patterns for  $6 \times 6$  and  $18 \times 3$  arrays along with a performance comparison in Section 5, followed by a conclusion in Section 6.

## 2. Mathematical Modeling of PV Modules and Arrays

The work begins with the modeling of PV modules based on the single-diode electrical circuit, as presented in Figure 1, which contains a current-generating source, cells connected in series ( $N_S$ ) and parallel ( $N_P$ ), series resistance ( $R_S$ ), and parallel resistance ( $R_P$ ). The current output can be established by applying Kirchhoff's current law in the circuit, and can be given as

$$I = N_P I_{PV} - N_P I_0 \left[ \exp \left\{ \frac{q(V_M + I R_S \left( \frac{N_S}{N_P} \right))}{\alpha K T N_S} \right\} - 1 \right] - \left[ \frac{V_M + I R_S \left( \frac{N_S}{N_P} \right)}{R_P \left( \frac{N_S}{N_P} \right)} \right] \quad (1)$$

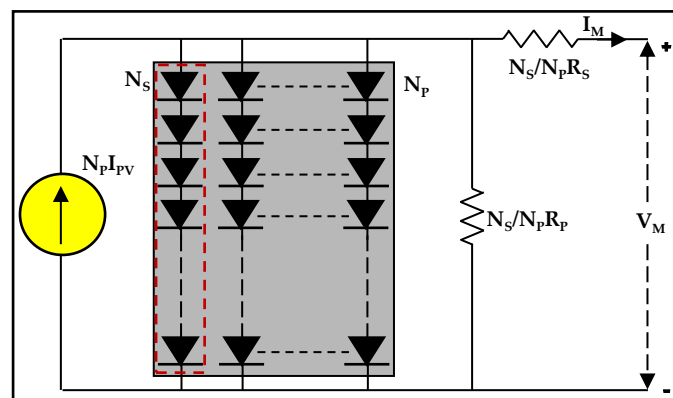


Figure 1. Circuit representation of PV modules.

The cell current is represented as  $I_{PV}$ , with maximum voltage and current outputs being denoted by  $V_M$  and  $I_M$ , respectively. The parameters  $T$ ,  $q$ ,  $K$ ,  $I_0$  and  $\alpha$  represent the module temperature (in Kelvin), electron charge ( $1.6 \times 10^{-19}$  C), Boltzmann constant ( $1.3806 \times 10^{-23}$  J/K), reverse saturation current, and ideality factor, respectively. The value of  $I_{PV}$  in the above can be calculated using Equation (2), which shows the dependence of the current on the receiving irradiance with symbols  $I_{SC}$ ,  $S$ ,  $S_s$ ,  $c_i$ , and  $T_s$  are denoted as the



short-circuit current, irradiance, standard irradiance ( $1000 \text{ W/m}^2$ ), coefficient of current and standard temperature (298 K), respectively.

$$I_{PV} = \left( \frac{S}{S_S} \right) [I_{SC} + c_i(T - T_S)] \quad (2)$$

The module ratings are determined based on the performance under standard testing conditions, with an irradiance of  $1000 \text{ W/m}^2$  and a module temperature of  $25^\circ\text{C}$ . The maximum power, maximum voltage, open-circuit voltage, maximum current, short-circuit current and the area receiving irradiance of the PV module used under standard conditions are 325 W, 37.80 V, 46.60 V, 8.60 A, 9.20 A and  $1.69 \text{ m}^2$ , respectively.

To generate the required power, modules are connected in combination in series and parallel, forming an array that increases the terminal voltage and output current of the system. Additionally, the modules are connected in various other combinations derived from the series–parallel configuration in order to achieve higher performance under partial shading conditions, as explained in Section 3.

The performance of the PV arrays is evaluated using various mathematical parameters, including power–voltage (P–V) characteristic curves, maximum power output, mismatch loss, power reduction, power increment, efficiency, and performance index, the formulations of which are explained below.

The maximum power output ( $P_O$ ) is the main parameter used to calculate other parameters such as mismatch loss, power reduction, power increment, efficiency, and performance index, and the equations involved in the calculation are given in Equation (3), where  $P_T$ ,  $P_{US}$ ,  $P_{OX}$  and  $A$  denote the total available power, power with no shading, and power output for other configurations and areas, respectively.

$$\left. \begin{aligned} \text{Mismatch Loss (ML)} &= P_T - P_O \\ \text{Power Reduction (PR)} &= P_{US} - P_O \\ \text{Power Increment (PI)} &= \left( \frac{P_O - P_{OX}}{P_{OX}} \right) \times 100 \\ \text{Efficiency (E)} &= \frac{P_O}{S \times A \times \text{Number of Modules}} \times 100 \\ \text{Performance Index} &= \frac{P_O}{P_{US}} \times 100. \end{aligned} \right\} \quad (3)$$

### 3. PV Array Configurations: Conventional and Hybrid

The PV array configurations are the connection schemes between the modules, and are based on the addition of additional wires to the junctions of series–parallel-connected modules in order to provide an additional path through which the module currents can flow. These configurations are highly effective at mitigating the power loss in PV arrays during partial shading, and are classified into two categories, i.e., conventional and hybrid configurations. The power, voltage and current output ratings of these array configurations remain the same as the number of modules, and the initial electrical architecture remains the same.

#### 3.1. Conventional Configurations

The conventional array configuration used thus far is series–parallel connection, whereby the modules are connected in series for voltage increment, forming a string, and similar strings are connected in parallel for the current increment of the system. Subsequently, considering the partial shading effect and the power losses in the PV array, additional configurations were formed by connecting wires to the connection junctions of the modules, which were referred to as bridge-linked, honeycomb, and total-cross-tied, denoted by BL, HC and TCT, respectively. The schematic representation of the conventional configurations for a  $6 \times 6$  PV array is shown in Figure 2. Among these configurations, the TCT has been proved to be effective; however, other configurations have also been reported in some cases.

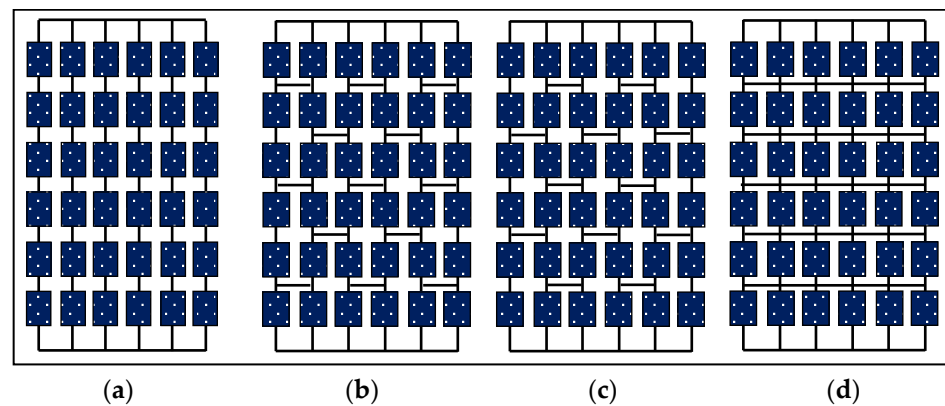


**Figure 2.** Conventional configurations for  $6 \times 6$  array. (a) Series-parallel, (b) bridge-Linked, (c) honeycomb, and (d) total-cross-tied.

### 3.2. Hybrid Configurations

Despite the higher power generation capability of the conventional configurations, the requirement of additional wires adds connection complexity, mainly in the case of large-sized PV arrays. Hence, various other configurations for the array from the combination of conventional configurations have been developed, as shown in Figure 3. The configurations were named according to the configurations combined to produce them, for example, the hybrid configuration for the series-parallel and total-cross-tied combination is named SP-TCT. Similarly, the combinations of bridge-linked and total-cross-tied, honeycomb and total-cross-tied, and bridge-linked and honeycomb are termed BL-TCT, HC-TCT and BL-HC, respectively.

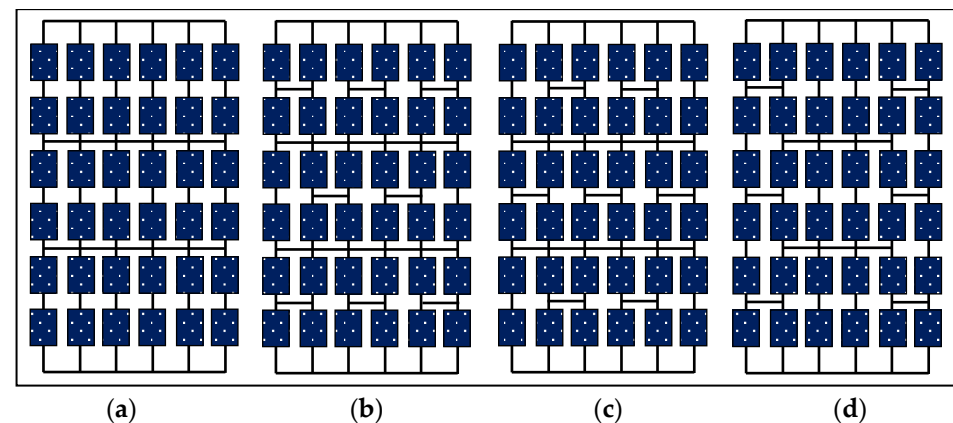


**Figure 3.** Hybrid configurations for  $6 \times 6$  PV array. (a) SP-TCT, (b) BL-TCT, (c) HC-TCT, and (d) BL-HC.

## 4. Two-Step Approach of Module Placement for PV Arrays

The proposed two-step approach is a module placement methodology for PV arrays in which the modules are repositioned using a certain technique to facilitate shade dispersion and increase the output power under partial shading conditions. The approach uses a fixed architecture along with a total-cross-tied electrical connection and requires no switches, sensors, complex algorithms, or dynamic parts, thus adding the advantage of easy implementation in PV arrays. The proposed technique uses a two-step module placement approach, a graphical representation of which is provided in Figure 4, where a  $6 \times 6$  PV array is taken as an example to perform the two-step approach for module replacement. The technique begins with an initial consideration of the PV modules numbered according to their row and column indices; for example, 34 denotes the modules located in the third row and fourth column of the array. The steps involved in the proposed technique do not

require the use of an algorithm, but can be executed using a simple mathematical procedure, as described below.

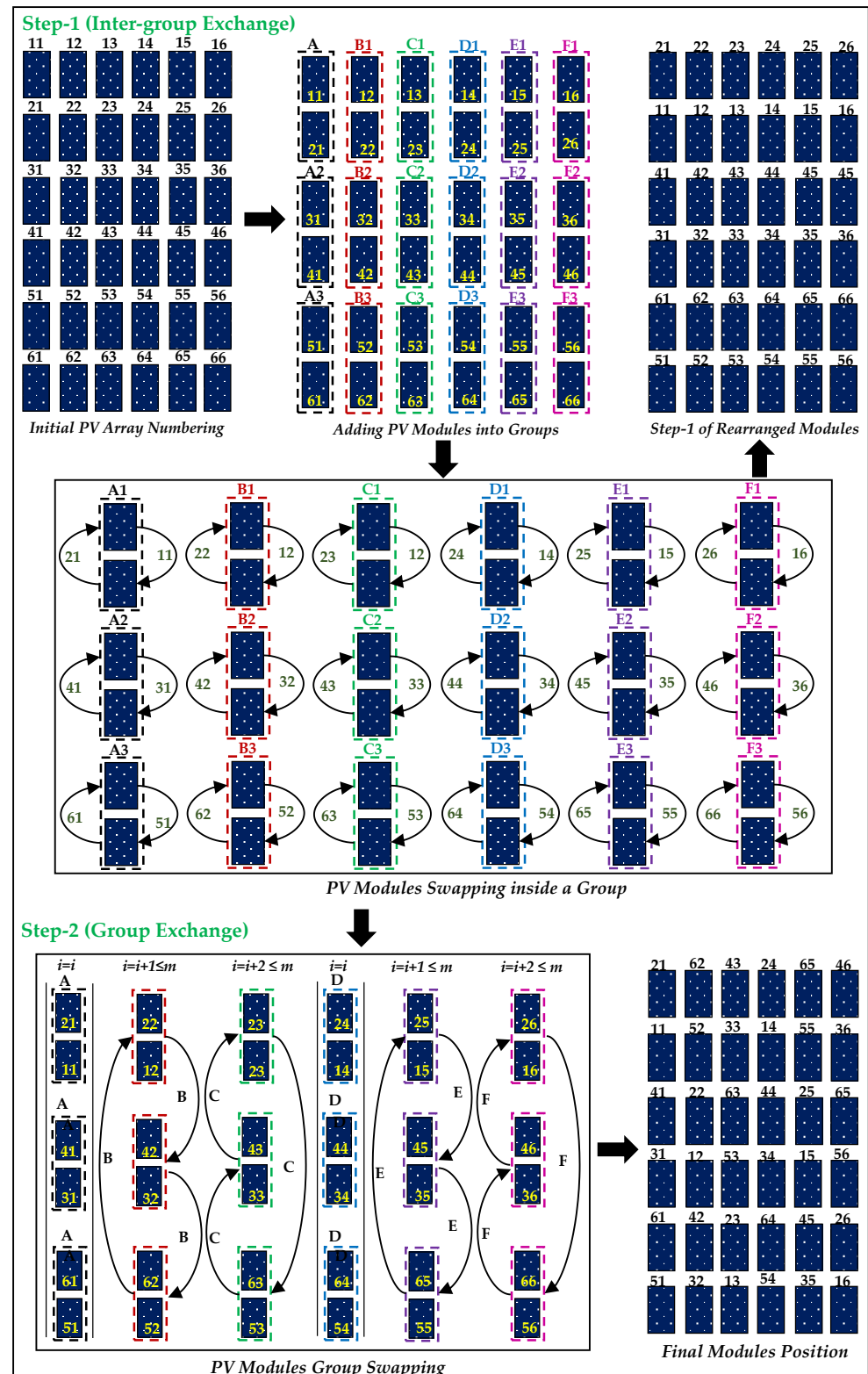


**Figure 4.** Graphical representation of the steps involved in the proposed two-step approach to module placement in the PV array.

**Step-1 (Inter-Group Exchange):** Initially, the array is divided into multiple groups with two modules in each group, with the nomenclature being A1, A2 and A3 for the first column, B1, B2 and B3 for the second column, C1, C2 and C3 for the third column, and so on. Then, the modules of the group are interchanged; for example, in group A1, module 11 takes the place of module 21, and vice versa. Considering another example, in group D3, modules 54 and 64 are interchanged, with 64 taking the place of 54, and vice-versa. In this manner, all the modules in the groups shown in Figure 4 (under step-1 analysis) are interchanged, resulting in a final rearranged PV array.

**Step-2 (Group Exchange):** In this step, the groups are now exchanged on the basis of a simple mathematical technique that allows proper dispersion of the shading. For column 1, all of the groups remain unaltered at their original position, and for column 2, the groups are shifted an additional one position, followed by an additional three positions for the groups in column 3. Again, this procedure is repeated for the next column, i.e., column 4, where the groups remain unaltered, followed by one additional shift for column 5, two additional shifts for column 6, and so on. This logic can be expressed as follows:

if  
 'n' represents the column of the array, 'm' states the total groups count and 'i' denotes the initial positions of the groups  
 then  
 for  $n = 1, i = 1$ , i.e., the groups remain altered  
 for  $n = 2, i = i + 1 \leq m$  (if not, then  $i = m - i$ ), i.e., additional one shifting  
 for  $n = 3, i = i + 2 \leq m$  (if not, then  $i = m - i$ ), i.e., additional two shifting  
 for  $n = 4, i = 1$ , i.e., the groups remain altered  
 for  $n = 5, i = i + 1 \leq m$  (if not, then  $i = m - i$ ), i.e., additional one shifting  
 and so on.

Considering the example for a  $6 \times 6$  PV array shown in Figure 4, the groups of the first column (A1, A2 and A3) remain at their original position. For the second column, the groups are shifted to the positions  $i + 1$ , i.e., group B1 with the initial position ( $i$ ) as 1 is shifted to the  $i + 1 = 1 + 1 = 2$ nd position ( $< 3$ ), taking the place of B2, and B2 ( $i = 2$ ) moves to the third position ( $i + 1 = 2 + 1 = 3 \leq 3$ ). For B3 ( $i = 3$ ), as the updated value of 'i' was calculated to be  $i + 2 = 3 + 2 = 5$ , which is greater than  $m = 3$ , the recalculation is performed, i.e.,  $i = m - i = 3 - 3 = 1$ , i.e., the group is shifted to the first position. Similarly, the process continues for the third column (C1, C2 and C3) and repeats from the fourth (D1, D2 and D3) column to the sixth column (F1, F2 and F3). The final array with the two-step approach of module shifting is depicted in Figure 4 (under step-2 analysis), which is considered to be the final architecture based on which the modules are replaced. Citing an example of the final  $6 \times 6$  array, it can be observed that in the first column, the initial module 11 is shifted to the position of 21, and vice-versa; initial module 31 is shifted to the position of 41, and vice-versa; and initial module 51 is shifted to the position of 61, and vice versa. For the second column, the modules 12, 22, 32, 42, 52 and 62 are shifted to the positions of 42, 32, 62, 52, 22 and 12, respectively, and so on. It has to be noted that the electrical connection remains the same as in the cases of a total-cross-tied connection, and hence, the electrical parameters remain equal to those of other configurations. In the case of an odd row count, the last single module can be treated as a single group, and the procedure continues according to the given methodology. Additionally, the proposed methodology is not limited to symmetric arrays, but have a wide range of applications in arbitrarily sized arrays. Some examples of other array sizes based on the two-step approach of module placement are pictorially represented in Figure 5. It is to be noted that the two-step technique is a module placement technique in which the electrical connection of the modules remains equivalent to that of the total-cross-tied connection; therefore, the electrical wiring and wiring length remain the same as that of the total-cross-tied array. Additionally, in practical applications, the array can experience a loss of 1–2% due to wires, but for the purposes of simulation validation, such losses are excluded in this study.

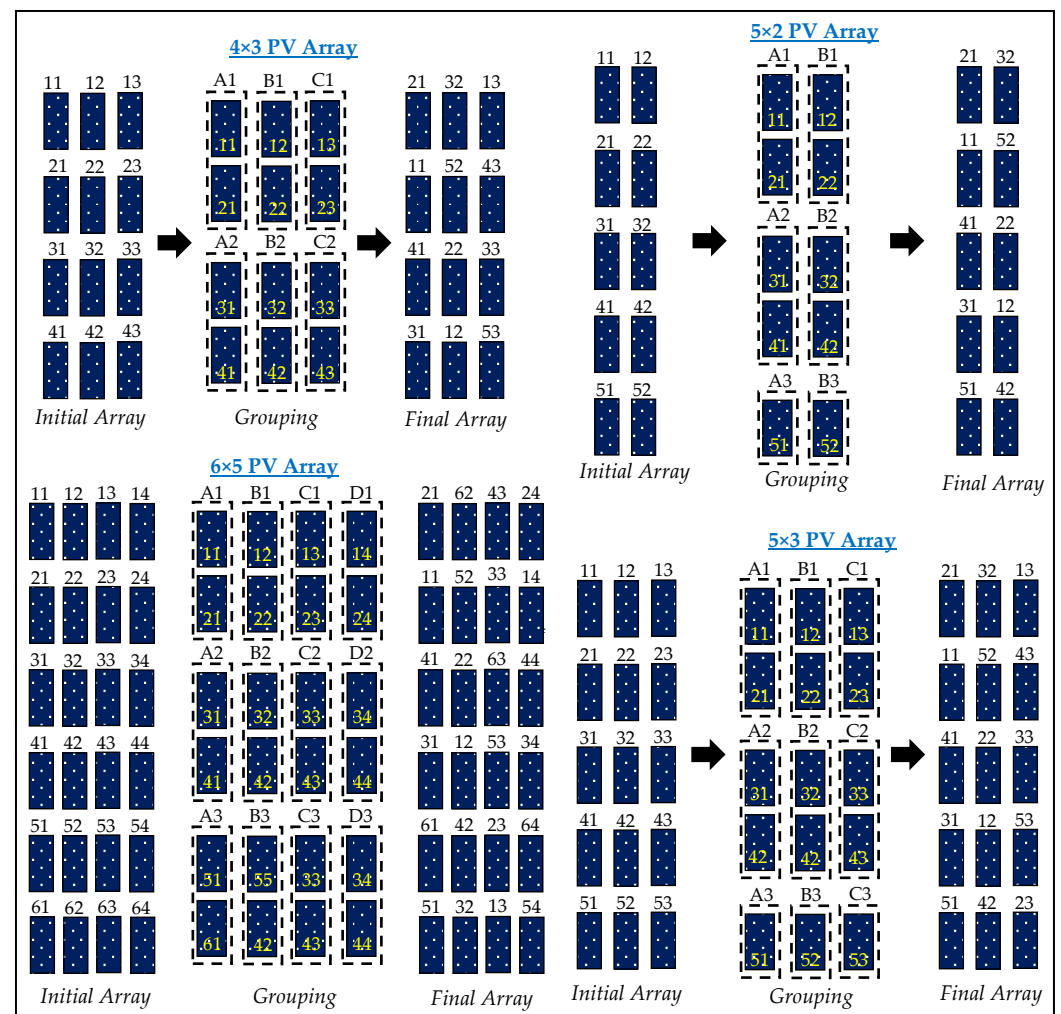


Figure 5. Application of the proposed two-step approach in arbitrary PV array sizes.

## 5. Analysis under Partial Shading (Results and Discussion)

The proposed two-step approach was implemented in two array sizes, i.e., symmetric ( $6 \times 6$ ) and asymmetric ( $18 \times 3$ ), and tested under numerous actual and random shading scenarios. The shade dispersion ability of the proposed methodology was validated on the basis of a comparison with conventional (SP, BL, HC and TCT) and hybrid (SP-TCT, BL-TCT, HC-TCT and BL-HC), along with the static electrical reconfiguration technique. The evaluation of the performance was carried out on the basis of the power–voltage ( $P$ – $V$ ) curves, power generation, mismatch loss, power reduction, power increment, efficiency and performance index, the mathematical formulations of which are given in Equation (3).

### 5.1. Symmetric $6 \times 6$ PV Array

The  $6 \times 6$  PV array has the maximum power output of 9.58 kW when all modules are operating under  $800 \text{ W/m}^2$  irradiance and  $50^\circ\text{C}$  module temperature, which reflects the no-shading situation. The evaluation was conducted by considering numerous partial shading situations based on actual cases and random situations. The partial shading cases based on the actual cases used in the study for the PV arrays are pictorially presented in Figure 6. It has to be noted that all the shading cases used for testing differ from each other in terms of location, area, pattern and irradiance levels.



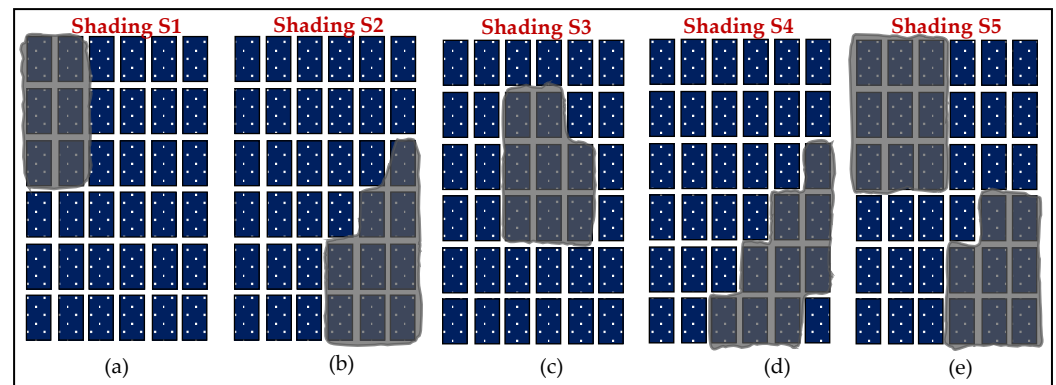


**Figure 6.** Partial shadings (a) S1, (b) S2, (c) S3, (d) S4, and (e) S5 for testing in PV arrays (based on actual cases).

#### 5.1.1. Evaluation under Partial Shading S1

The blocks showing the irradiance levels of the PV array during partial shading S1 (Figure 6a) are shown in Figure 7, where the partial shading reduced the received irradiance of the modules from  $800 \text{ W/m}^2$  ( $50^\circ\text{C}$ ) to  $100 \text{ W/m}^2$  ( $53^\circ\text{C}$ ) and  $150 \text{ W/m}^2$  ( $52.6^\circ\text{C}$ ). As the conventional and hybrid configurations have no shading dispersion capability, the block for total-cross-tied (TCT) represents the irradiance levels for all.

Total-Cross-Tied						Static Electrical Reconfiguration						Two-Step Approach					
100	150	800	800	800	800	100	800	800	800	800	800	100	800	800	800	800	800
100	150	800	800	800	800	100	150	800	800	800	800	100	800	800	800	800	800
100	150	800	800	800	800	100	150	800	800	800	800	800	150	800	800	800	800
800	800	800	800	800	800	800	150	800	800	800	800	800	100	150	800	800	800
800	800	800	800	800	800	800	800	800	800	800	800	800	800	800	800	800	800
800	800	800	800	800	800	800	800	800	800	800	800	800	800	800	800	800	800
(a)						(b)						(c)					

**Figure 7.** Irradiance received by the  $6 \times 6$  PV array during partial shading S1 for (a) conventional, hybrid and TCT, (b) static electrical reconfiguration (shade dispersion), and (c) the two-step approach (shade dispersion).

As most of this analysis demonstrated the increased effectiveness of the TCT over the other configurations, the mathematical comparison of power output was performed with TCT. For partial shading S1 in an array with TCT, the current output by different rows based on the irradiance block in Figure 7a was calculated as follows:

$$\left. \begin{aligned} I_{\text{Row1}} &= \frac{100}{1000} I_M + \frac{150}{1000} I_M + \frac{800}{1000} I_M + \frac{800}{1000} I_M + \frac{800}{1000} I_M + \frac{800}{1000} I_M = 3.45 I_M \\ I_{\text{Row2}} &= \frac{100}{1000} I_M + \frac{150}{1000} I_M + \frac{800}{1000} I_M + \frac{800}{1000} I_M + \frac{800}{1000} I_M + \frac{800}{1000} I_M = 3.45 I_M \\ I_{\text{Row3}} &= \frac{100}{1000} I_M + \frac{150}{1000} I_M + \frac{800}{1000} I_M + \frac{800}{1000} I_M + \frac{800}{1000} I_M + \frac{800}{1000} I_M = 3.45 I_M \\ I_{\text{Row4}} &= \frac{800}{1000} I_M + \frac{800}{1000} I_M + \frac{800}{1000} I_M + \frac{800}{1000} I_M + \frac{800}{1000} I_M + \frac{800}{1000} I_M = 4.8 I_M \\ I_{\text{Row5}} &= \frac{800}{1000} I_M + \frac{800}{1000} I_M + \frac{800}{1000} I_M + \frac{800}{1000} I_M + \frac{800}{1000} I_M + \frac{800}{1000} I_M = 4.8 I_M \\ I_{\text{Row6}} &= \frac{800}{1000} I_M + \frac{800}{1000} I_M + \frac{800}{1000} I_M + \frac{800}{1000} I_M + \frac{800}{1000} I_M + \frac{800}{1000} I_M = 4.8 I_M \end{aligned} \right\} \quad (4)$$

The mathematical current estimation for the static electrical reconfiguration using the irradiance block presented in Figure 7b was calculated using Equation (5).

$$\left. \begin{aligned} I_{Row3} &= \frac{100}{1000} I_M + \frac{150}{1000} I_M + \frac{800}{1000} I_M + \frac{800}{1000} I_M + \frac{800}{1000} I_M + \frac{800}{1000} I_M = 4.1 I_M \\ I_{Row4} &= \frac{800}{1000} I_M + \frac{800}{1000} I_M + \frac{800}{1000} I_M + \frac{800}{1000} I_M + \frac{800}{1000} I_M + \frac{800}{1000} I_M = 3.45 I_M \\ I_{Row5} &= \frac{800}{1000} I_M + \frac{800}{1000} I_M + \frac{800}{1000} I_M + \frac{800}{1000} I_M + \frac{800}{1000} I_M + \frac{800}{1000} I_M = 3.45 I_M \\ I_{Row6} &= \frac{800}{1000} I_M + \frac{800}{1000} I_M + \frac{800}{1000} I_M + \frac{800}{1000} I_M + \frac{800}{1000} I_M + \frac{800}{1000} I_M = 4.15 I_M \\ I_{Row1} &= \frac{100}{1000} I_M + \frac{800}{1000} I_M + \frac{800}{1000} I_M + \frac{800}{1000} I_M + \frac{800}{1000} I_M + \frac{800}{1000} I_M = 4.8 I_M \\ I_{Row1} &= \frac{100}{1000} I_M + \frac{800}{1000} I_M + \frac{800}{1000} I_M + \frac{800}{1000} I_M + \frac{800}{1000} I_M + \frac{800}{1000} I_M = 4.8 I_M \end{aligned} \right\} \quad (5)$$

For the two-step approach, the irradiance block in Figure 7c was used to estimate the current output of the array calculated in Equation (6).

$$\left. \begin{aligned} I_{Row1} &= \frac{100}{1000} I_M + \frac{800}{1000} I_M + \frac{800}{1000} I_M + \frac{800}{1000} I_M + \frac{800}{1000} I_M + \frac{800}{1000} I_M = 4.1 I_M \\ I_{Row2} &= \frac{100}{1000} I_M + \frac{800}{1000} I_M + \frac{800}{1000} I_M + \frac{800}{1000} I_M + \frac{800}{1000} I_M + \frac{800}{1000} I_M = 4.1 I_M \\ I_{Row3} &= \frac{800}{1000} I_M + \frac{150}{1000} I_M + \frac{800}{1000} I_M + \frac{800}{1000} I_M + \frac{800}{1000} I_M + \frac{800}{1000} I_M = 4.15 I_M \\ I_{Row4} &= \frac{100}{1000} I_M + \frac{150}{1000} I_M + \frac{800}{1000} I_M + \frac{800}{1000} I_M + \frac{800}{1000} I_M + \frac{800}{1000} I_M = 3.45 \\ I_{Row5} &= \frac{800}{1000} I_M + \frac{800}{1000} I_M + \frac{800}{1000} I_M + \frac{800}{1000} I_M + \frac{800}{1000} I_M + \frac{800}{1000} I_M = 4.8 I_M \\ I_{Row6} &= \frac{800}{1000} I_M + \frac{150}{1000} I_M + \frac{800}{1000} I_M + \frac{800}{1000} I_M + \frac{800}{1000} I_M + \frac{800}{1000} I_M = 4.15 I_M \end{aligned} \right\} \quad (6)$$

The mathematical estimations of the current, voltage and power outputs for different rows of TCT, static electrical reconfiguration and the two-step approach are summarized in Table 1. It can be seen that TCT, static electrical reconfiguration and the two-step approach have a mathematically equal estimated power output value of  $20.7 V_M I_M$ ; however, by viewing the current output values of the rows, it can be seen that there is a minimum current difference between the rows in the case of the two-step approach. The validation of the effective shade dispersion by the proposed two-step approach was further performed using P-V curve analysis and parameter comparison with other configurations.

The total available power of the array during partial shading S1 was calculated to be 8.17 kW, on the basis of which the power output of the SP, BL, HC, TCT, SP-TCT, BL-TCT, HC-TCT and BL-HC were determined to be 7.08 kW, 7.08 kW, 7.14 kW, 7.34 kW, 7.23 kW, 7.25 kW, 7.22 kW and 7.18 kW, respectively. Static electrical reconfiguration generated a higher power output of 7.40 kW than the conventional and hybrid configurations; however, the two-step approach presented a maximum power output of 7.52 kW, representing a 6.21%, 6.21%, 5.32%, 2.45%, 4.01%, 3.72%, 4.15%, 4.73% and 1.63% increment in power compared to SP, BL, HC, TCT, SP-TCT, BL-TCT, HC-TCT, BL-HC and static electrical reconfiguration, respectively. On the basis of the parameter calculation formulas given in Equation (3), the mismatch loss and power reduction experienced when using the two-step approach were calculated and found to have lower values of 0.65 kW and 2.05 kW, respectively. Additionally, there is an increase in the values of efficiency and performance index of 15.39% and 78.57% when using the two-step approach compared to when using the other configurations. Among all of the configurations, the SP showed the poorest performance and suffered higher mismatch loss (1.09 kW) and power reduction (2.49 kW) with lower efficiency (14.49%) and performance index (73.98%). The comparison of the P~V curve of the array with the proposed two-step approach for partial shading S1 with the conventional (SP, BL, HC and TCT), hybrid (SP-TCT, BL-TCT, HC-TCT, BL-HC) and static electrical reconfiguration is graphically presented in Figure 8a, 8b and 8c, respectively. Additionally, a comparison of the configurations in terms of different parameters was performed through bar graph analysis, as given in Figure 8d. On the basis of the graphical results, it can be observed that the proposed approach performed well during partial shading S1, and can be stated to be the best technique for power enhancement. Additionally, the arrays were operated under the same shading case by maintaining the temperature of all modules at 50 °C, and it was observed that the power generation remained nearly the same as that in the varying temperature case. The average power difference under constant temperature and varying temperature cases under partial shading was determined to be 0.019 W, which

is much less than the total array rating. On the basis of this analysis, it can be stated that module temperature has a minimal effect on the power generation of the array during partial shading, and therefore, temperature variation was considered in this study.

**Table 1.** Summarized mathematical estimation of the current, voltage and power values of the PV array under partial shading S1.

Array with Total-Cross-Tied						
	Row 1	Row 2	Row 3	Row 4	Row 5	Row 6
Row Currents	3.45 $I_M$	3.45 $I_M$	3.45 $I_M$	4.80 $I_M$	4.80 $I_M$	4.80 $I_M$
Row Voltages	6 $V_M$	5 $V_M$	4 $V_M$	3 $V_M$	2 $V_M$	$V_M$
Row Powers	20.7 $V_M I_M$	17.25 $V_M I_M$	13.8 $V_M I_M$	14.4 $V_M I_M$	9.60 $V_M I_M$	4.80 $V_M I_M$
Array with Static Electrical Reconfiguration						
	Row 2	Row 3	Row 1	Row 4	Row 5	Row 6
Row Currents	3.45 $I_M$	3.45 $I_M$	4.10 $I_M$	4.15 $I_M$	4.80 $I_M$	4.80 $I_M$
Row Voltages	6 $V_M$	5 $V_M$	4 $V_M$	3 $V_M$	2 $V_M$	$V_M$
Row Powers	20.7 $V_M I_M$	17.25 $V_M I_M$	16.4 $V_M I_M$	12.45 $V_M I_M$	9.60 $V_M I_M$	4.80 $V_M I_M$
Array with Two-Step Approach						
	Row 4	Row 3	Row 6	Row 1	Row 2	Row 5
Row Currents	3.45 $I_M$	4.10 $I_M$	4.10 $I_M$	4.10 $I_M$	4.15 $I_M$	4.80 $I_M$
Row Voltages	6 $V_M$	5 $V_M$	4 $V_M$	3 $V_M$	2 $V_M$	$V_M$
Row Powers	20.7 $V_M I_M$	20.5 $V_M I_M$	16.4 $V_M I_M$	12.3 $V_M I_M$	8.30 $V_M I_M$	4.80 $V_M I_M$

Green and red Color indicates the highest and lowest power output of the PV array.

### 5.1.2. Evaluation under Partial Shading S2

The irradiance block for the TCT, conventional and hybrid configurations, static electrical reconfiguration and the two-step approach for partial shading S2 (Figure 6b) are shown in Figure 9a,b,c, respectively. It can be observed that the partially shaded modules have four irradiance values—200 W/m<sup>2</sup>, 250 W/m<sup>2</sup>, 300 W/m<sup>2</sup> and 350 W/m<sup>2</sup>—along with 800 W/m<sup>2</sup> for the unshaded modules. The summarized mathematical estimation values for currents, voltages, and powers of rows for TCT, static electrical reconfiguration and the proposed two-step approach are tabulated in Table 2. From the mathematical calculations, it can be observed that the two-step approach has a higher mathematical power value of 21.6  $V_M I_M$ , whereas the static reconfiguration and TCT have 18.90  $V_M I_M$  and 18  $V_M I_M$ , respectively. The total available power output of the array was theoretically calculated to be 7.91 kW.

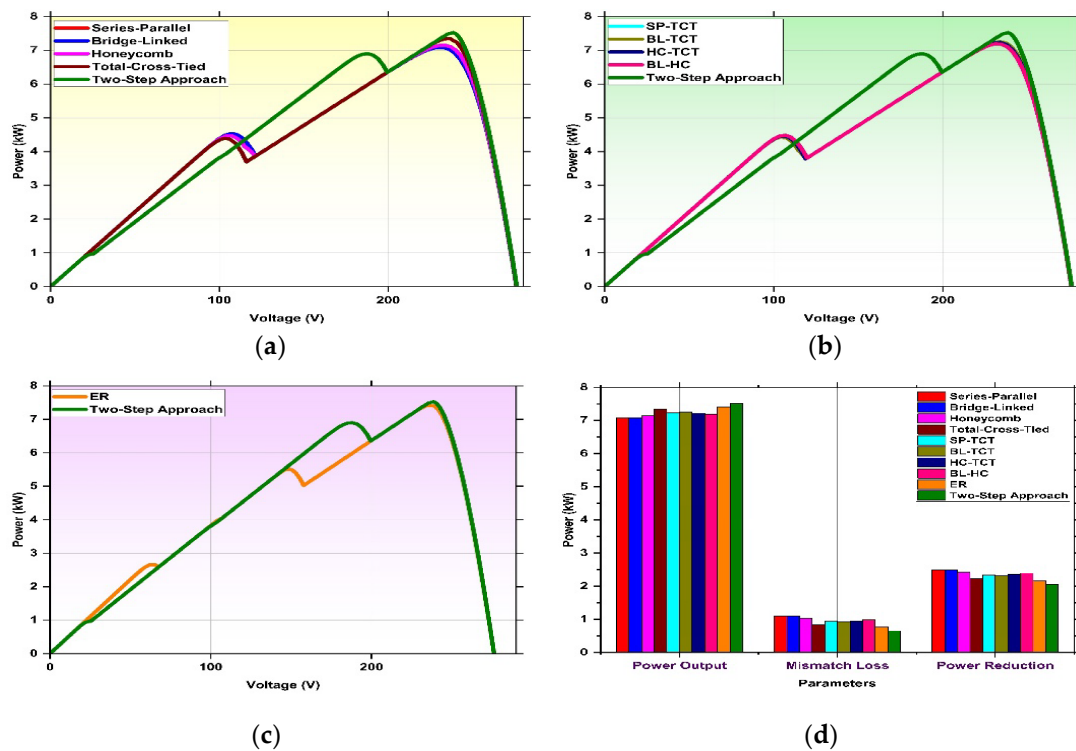


**Figure 8.** Graphical comparison of two-step approach under partial shading S1. (a) P~V curve comparison with conventional configurations, (b) P~V curve comparison with hybrid configurations, (c) P~V curve comparison with the static reconfiguration technique, and (d) comparison of the parameters among all configurations.

Total-Cross-Tied						Static Electrical Reconfiguration						Two-Step Approach					
800	800	800	800	800	800	800	800	800	800	800	800	800	800	800	200	300	300
800	800	800	800	800	800	800	800	800	250	300	350	800	800	800	800	250	350
800	800	800	800	800	350	800	800	800	200	250	300	800	800	800	800	800	200
800	800	800	800	300	300	800	800	800	800	200	250	800	800	800	800	800	250
800	800	800	250	250	250	800	800	800	800	800	200	800	800	800	200	300	800
800	800	800	200	200	200	800	800	800	800	800	800	800	800	800	250	800	800

**Figure 9.** Irradiance received by the  $6 \times 6$  PV array during partial shading S2 for (a) conventional, hybrid and TCT, (b) static electrical reconfiguration (shade dispersion), and (c) the two-step approach (shade dispersion).

The power output achieved when using the two-step approach was notably higher, with a value equal to 7.78 kW, whereas the SP has a value of 6.19 kW, along with 6.39 kW for BL, 6.49 kW for HC, 6.63 kW for TCT, 6.57 kW for SP-TCT, 6.59 kW for BL-TCT, 6.57 kW for HC-TCT, 6.51 kW for BL-HC and 6.90 kW for static reconfiguration.

Additionally, the P~V curve comparisons of the two-step approach with the conventional, hybrid and static reconfiguration presented in Figure 10a,b,c, respectively, show that the proposed technique offers a higher power output than the others. The mismatch losses of the SP, BL, HC, TCT, SP-TCT, BL-TCT, HC-TCT, BL-HC and static configurations were calculated to be 1.7 kW, 1.52 kW, 1.42 kW, 1.28 kW, 1.34 kW, 1.32 kW, 1.34 kW, 1.4

kW and 1.01 kW, values which are higher than that obtained when using the proposed approach, which was 0.13 kW. Additionally, the power reduction was found to be lower when using the two-step approach (1.79 kW) than when using SP (3.38 kW), BL (3.18 kW), HC (3.08 kW), TCT (2.94 kW), SP-TCT (3 kW), BL-TCT (2.98 kW), HC-TCT (3 kW), BL-HC (3.06 kW) or static reconfiguration (2.67 kW). The efficiencies of the SP, BL, HC, TCT, SP-TCT, BL-TCT, HC-TCT, BL-HC, static reconfiguration and two-step approach were calculated to be 12.67%, 13.08%, 13.29%, 13.57%, 13.45%, 13.49%, 13.45%, 13.33%, 14.12% and 15.93%, respectively. The performance index of the array was calculated to be 64.68%, 66.77%, 67.81%, 69.29%, 68.65%, 68.86%, 68.65%, 68.02%, 72.10% and 81.29% for SP, BL, HC, TCT, SP-TCT, BL-TCT, HC-TCT, BL-HC, static reconfiguration and the two-step approach, respectively. On the basis of the parameter comparison graph given in Figure 10d, it can be observed that the two-step approach presented a higher performance than the other configurations, with 25.68%, 21.57%, 19.87%, 17.34%, 18.41%, 18.05%, 18.41%, 19.50% and 12.75% higher power output than SP, BL, HC, TCT, SP-TCT, BL-TCT, HC-TCT, BL-HC and static reconfiguration, respectively.

**Table 2.** Summarized mathematical estimation of current, voltage and power values of the PV array under partial shading S2.

Array with Total-Cross-Tied						
	Row 6	Row 5	Row 4	Row 3	Row 1	Row 2
Row Currents	3 $I_M$	3.15 $I_M$	3.8 $I_M$	4.35 $I_M$	4.80 $I_M$	4.80 $I_M$
Row Voltages	6 $V_M$	5 $V_M$	4 $V_M$	3 $V_M$	2 $V_M$	$V_M$
Row Powers	18 $V_M I_M$	15.75 $V_M I_M$	15.2 $V_M I_M$	13.05 $V_M I_M$	9.60 $V_M I_M$	4.80 $V_M I_M$
Array with Static Electrical Reconfiguration						
	Row 3	Row 2	Row 4	Row 5	Row 1	Row 6
Row Currents	3.15 $I_M$	3.30 $I_M$	3.65 $I_M$	4.20 $I_M$	4.80 $I_M$	4.80 $I_M$
Row Voltages	6 $V_M$	5 $V_M$	4 $V_M$	3 $V_M$	2 $V_M$	$V_M$
Row Powers	18.9 $V_M I_M$	16.50 $V_M I_M$	14.60 $V_M I_M$	12.60 $V_M I_M$	9.60 $V_M I_M$	4.80 $V_M I_M$
Array with Two-Step Approach						
	Row 1	Row 5	Row 2	Row 3	Row 4	Row 6
Row Currents	3.60 $I_M$	3.70 $I_M$	3.80 $I_M$	4.20 $I_M$	4.25 $I_M$	4.25 $I_M$
Row Voltages	6 $V_M$	5 $V_M$	4 $V_M$	3 $V_M$	2 $V_M$	$V_M$
Row Powers	21.6 $V_M I_M$	18.50 $V_M I_M$	15.20 $V_M I_M$	12.60 $V_M I_M$	8.50 $V_M I_M$	4.25 $V_M I_M$

Green and red Color indicates the highest and lowest power output of the PV array.

### 5.1.3. Evaluation under Partial Shading S3

The total power available in the PV array was calculated to be 8.48 kW for shading S3 (Figure 11) with the higher mathematical power generation of 24  $V_M I_M$  by static reconfiguration and two-step approach (Table 3). A graphical comparison of the two-step approach with the conventional and hybrid configurations along with static electrical reconfiguration in terms of P-V curves and parameters is presented in Figure 12. The maximum power output of SP, BL, HC, TCT, SP-TCT, BL-TCT, HC-TCT, BL-HC, static electrical reconfiguration



and two-step approach was determined to be 7.50 kW, 7.52 kW, 7.55 kW, 7.73 kW, 7.70 kW, 7.70 kW, 7.72 kW, 7.59 kW, 8.30 kW and 8.38 kW, respectively. The two-step approach had the lowest mismatch loss and power reduction, at 0.06 kW and 1.15 kW, respectively, along with a higher efficiency and performance index, at 17.24% and 87.98%, respectively. The power increment achieved when using the two-step approach was calculated to be 13.06%, 12.76%, 12.31%, 9.70%, 10.12%, 10.12%, 9.84%, 11.72% and 2.16%, respectively.

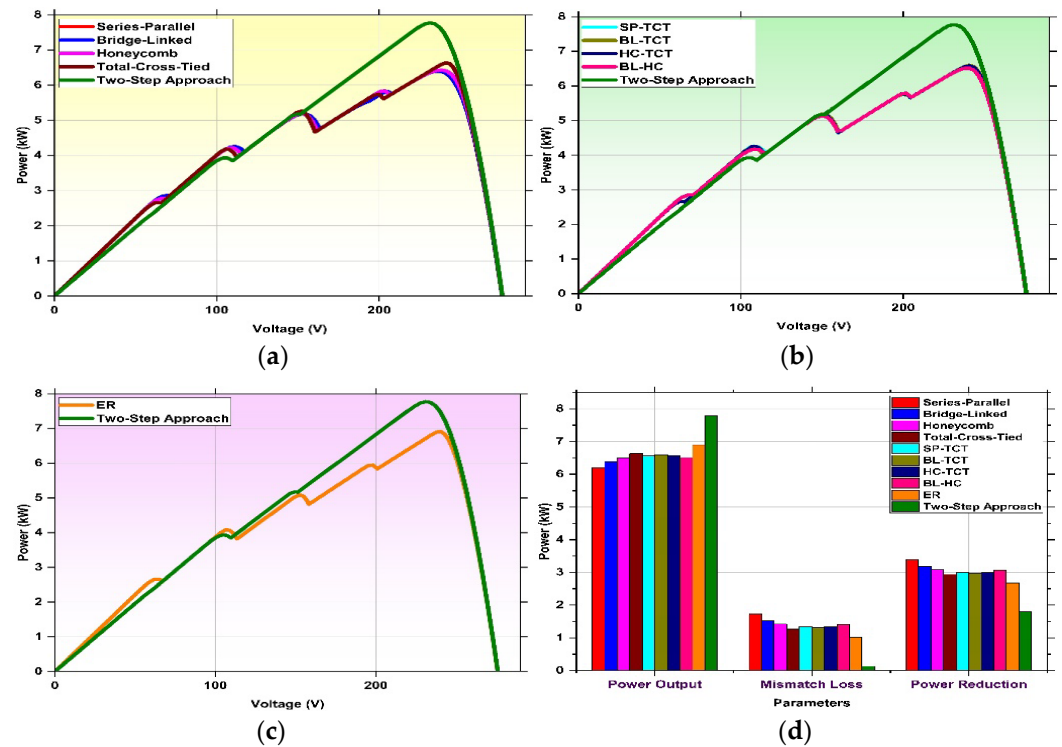


**Figure 10.** Graphical comparison of the two-step approach under partial shading S2. (a) P~V curve comparison with conventional configurations, (b) P~V curve comparison with hybrid configurations, (c) P~V curve comparison with the static reconfiguration technique, and (d) comparison of parameters among all configurations.

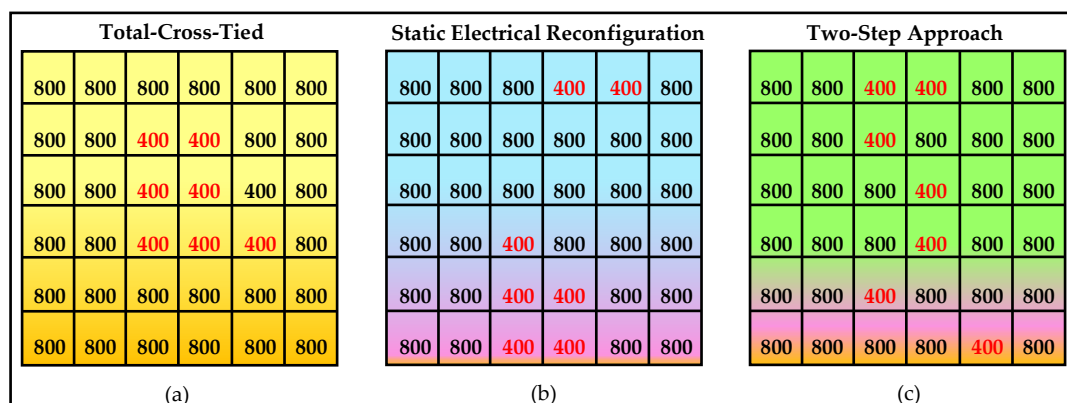


**Figure 11.** Irradiance received by the  $6 \times 6$  PV array during partial shading S3 for (a) conventional, hybrid and TCT, (b) static electrical reconfiguration (shade dispersion), and (c) the two-step approach (shade dispersion).

**Table 3.** Summarized mathematical estimation of the current, voltage and power values of the PV array under partial shading S3.

Array with Total-Cross-Tied						
	Row 4	Row 2	Row 3	Row 1	Row 5	Row 6
Row Currents	$3.6 I_M$	$4.0 I_M$	$4.0 I_M$	$4.8 I_M$	$4.8 I_M$	$4.8 I_M$
Row Voltages	$6 V_M$	$5 V_M$	$4 V_M$	$3 V_M$	$2 V_M$	$V_M$
Row Powers	$21.6 V_M I_M$	$20.0 V_M I_M$	$16.0 V_M I_M$	$14.4 V_M I_M$	$9.60 V_M I_M$	$4.80 V_M I_M$
Array with Static Electrical Reconfiguration						
	Row 3	Row 2	Row 4	Row 5	Row 1	Row 6
Row Currents	$4.0 I_M$	$4.0 I_M$	$4.0 I_M$	$4.4 I_M$	$4.8 I_M$	$4.8 I_M$
Row Voltages	$6 V_M$	$5 V_M$	$4 V_M$	$3 V_M$	$2 V_M$	$V_M$
Row Powers	$24 V_M I_M$	$20 V_M I_M$	$16 V_M I_M$	$13.2 V_M I_M$	$9.60 V_M I_M$	$4.80 V_M I_M$
Array with Two-Step Approach						
	Row 1	Row 5	Row 2	Row 3	Row 4	Row 6
Row Currents	$4.0 I_M$	$4.4 I_M$	$4.4 I_M$	$4.4 I_M$	$4.4 I_M$	$4.4 I_M$
Row Voltages	$6 V_M$	$5 V_M$	$4 V_M$	$3 V_M$	$2 V_M$	$V_M$
Row Powers	$24 V_M I_M$	$22 V_M I_M$	$17.6 V_M I_M$	$13.2 V_M I_M$	$8.8 V_M I_M$	$4.4 V_M I_M$

Green and red Color indicates the highest and lowest power output of the PV array.

#### 5.1.4. Evaluation under Partial Shading S4

The irradiance blocks of the array are shown in Figure 13, and the mathematical power output of the two-step approach, static reconfiguration and TCT were calculated to be  $25.8 V_M I_M$ ,  $22.8 V_M I_M$  and  $24 V_M I_M$ , respectively. The total power available in the array was calculated to be 8.85 kW, on the basis of which the power output by SP, BL, HC, TCT, SP-TCT, BL-TCT, HC-TCT, BL-HC, static reconfiguration and the two-step approach were determined to be 7.88 kW, 8 kW, 8.12 kW, 8.50 kW, 8.13 kW, 8.06 kW, 8.15 kW, 8.10 kW, 8.21 kW and 8.85 kW, respectively. The mismatch loss and power reduction in the two-step approach were calculated to be 0.56 kW and 0 kW, which is lower than for the other techniques. Comparisons of the P~V curves and the parameters of all of the configurations, static reconfiguration, and the two-step approach are shown in Figure 15a, from which it can be observed that the two-step approach has the higher values. The increment in power when using the two-step approach was calculated to be 12.30%, 10.63%, 8.99%, 4.11%, 8.85%, 9.80%, 8.58%, 9.25% and 7.79% for SP, BL, HC, TCT, SP-TCT, BL-TCT, HC-TCT, BL-HC and static reconfiguration, respectively.

#### 5.1.5. Evaluation under Partial Shading S5

The irradiance blocks of the array with conventional, hybrid and TCT, static reconfiguration, and the two-step approach are presented in Figure 14, and the maximum mathematical power outputs have been calculated to be  $16.2 V_M I_M$ ,  $11 V_M I_M$  and  $16.8 V_M I_M$ , respectively. The total power available in the array was calculated to be 5.86 kW, and the power output from SP, BL, HC, TCT, SP-TCT, BL-TCT, HC-TCT, BL-HC, static reconfiguration and the two-step approach was determined to be 4.42 kW, 3.70 kW, 3.87 kW, 5.71 kW,

4.78 kW, 4.78 kW, 4.77 kW, 4.77 kW, 4.02 kW and 5.85 kW, respectively. The performance of the two-step approach can be observed from the graphical comparison given in Figure 15b, in which the generated power output was 32.35%, 58.10%, 51.16%, 2.45%, 22.38%, 22.38%, 22.64%, 22.38% and 45.52% higher than that of SP, BL, HC, TCT, SP-TCT, BL-TCT, HC-TCT, BL-HC and static reconfiguration, respectively.

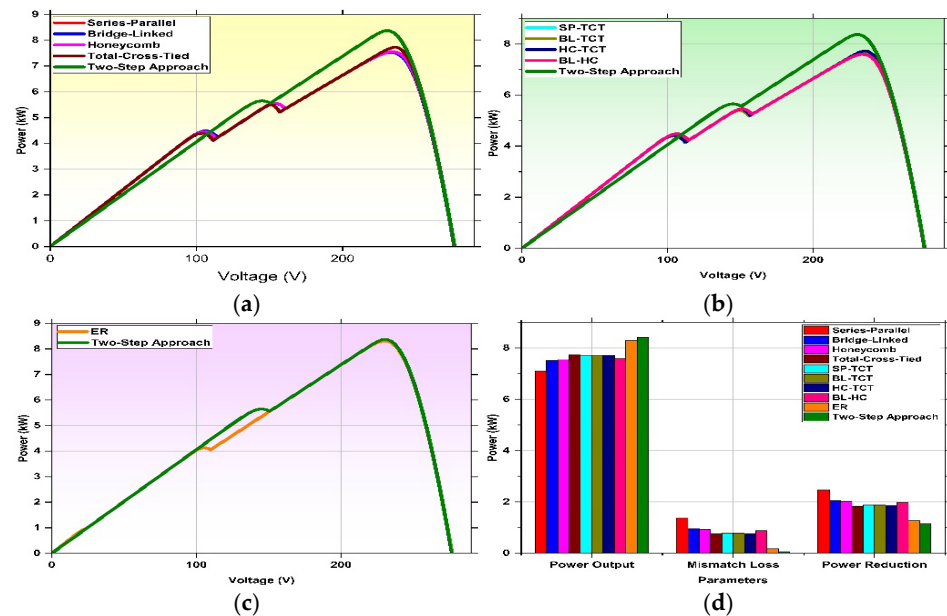


**Figure 12.** Graphical comparison of the two-step approach under partial shading S3. (a) P~V curve comparison with conventional configurations, (b) P~V curve comparison with hybrid configurations, (c) P~V curve comparison with the static reconfiguration technique, and (d) parameter comparison among all configurations.

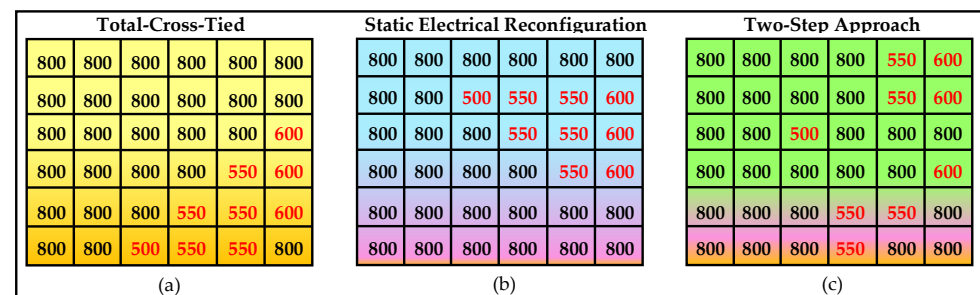


**Figure 13.** Irradiance received by the  $6 \times 6$  PV array during partial shading S4 for (a) conventional, hybrid and TCT, (b) static electrical reconfiguration (shade dispersion), and (c) the two-step approach (shade dispersion).

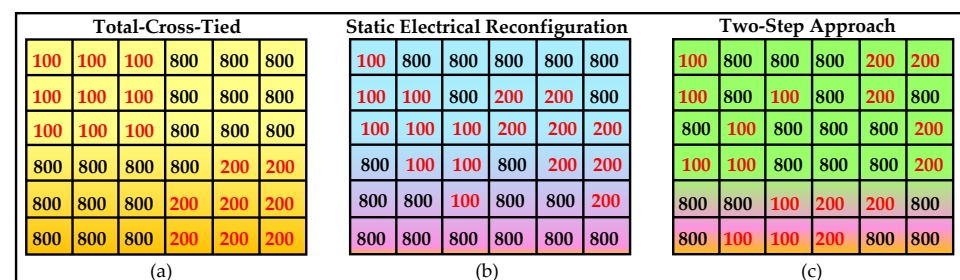


**Figure 14.** Irradiance received by the  $6 \times 6$  PV array during partial shading S5 for (a) conventional, hybrid and TCT, (b) static electrical reconfiguration (shade dispersion), and (c) the two-step approach (shade dispersion).

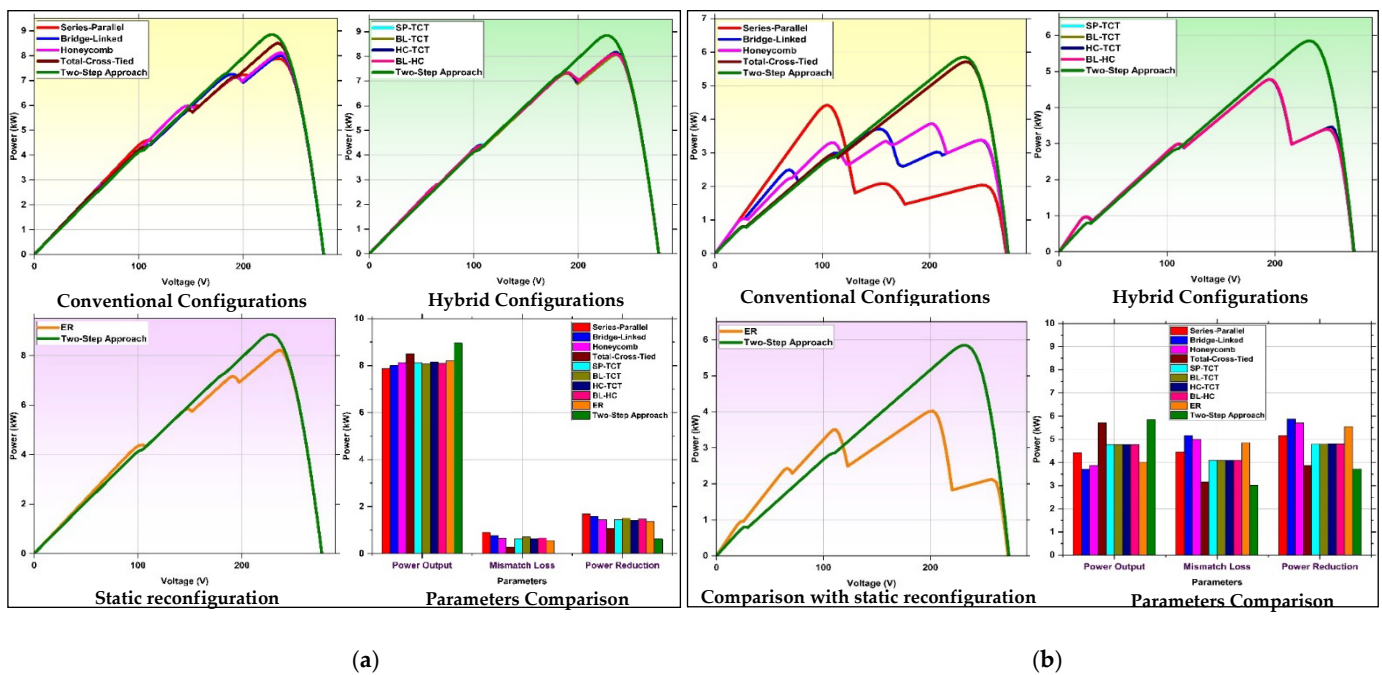


**Figure 15.** Graphical comparison of the two-step approach with conventional, hybrid configurations and static reconfiguration technique for partial shading: (a) S4 and (b) S5.

The summarized data for the different parameters of the conventional and hybrid configuration, static electrical reconfiguration, and the two-step approach for the five partial shading cases are given in Table 4.

Furthermore, the reliability of the proposed two-step approach was tested by applying various additional random partial shading patterns (as shown in Figure 16) in the  $6 \times 6$  array and comparing the power generation with the conventional, hybrid and static electrical reconfigurations. The  $P \sim V$  curves of the array for all the random partial shading cases are shown in Figure 17, from which it can be observed that the two-step approach has the highest power output. The detailed power output data of all the configurations for all the cases of partial shading are given in Table 5.

**Table 4.** Summarized data of the results obtained for the five partial shading cases.

Partial Shading S1					
Configuration	Power Output	ML	PR	E	P Index
SP	7.08 kW	1.09 kW	2.49 kW	14.49%	73.98%
BL	7.07 kW	1.09 kW	2.49 kW	14.49%	73.98%
HC	7.14 kW	1.03 kW	2.43 kW	14.62%	74.60%
TCT	7.34 kW	0.83 kW	2.23 kW	15.03%	76.69%
SP-TCT	7.23 kW	0.94 kW	2.34 kW	14.80%	75.54%
BL-TCT	7.25 kW	0.92 kW	2.32 kW	14.84%	75.75%
HC-TCT	7.22 kW	0.95 kW	2.35 kW	14.78%	75.44%
BL-HC	7.18 kW	0.99 kW	2.39 kW	14.70%	75.02%
Static Reconfiguration	7.40 kW	0.77 kW	2.17 kW	15.15%	77.32%
Two-Step Approach	7.52 kW	0.65 kW	2.05 kW	15.39%	78.57%

Table 4. Cont.

Partial Shading S2					
Configuration	Power Output	ML	PR	E	P Index
SP	6.19 kW	1.72 kW	3.38 kW	12.67%	64.68%
BL	6.39 kW	1.52 kW	3.18 kW	13.08%	66.77%
HC	6.49 kW	1.42 kW	3.08 kW	13.29%	67.81%
TCT	6.63 kW	1.28 kW	2.94 kW	13.57%	69.27%
SP-TCT	6.57 kW	1.34 kW	3 kW	13.45%	68.65%
BL-TCT	6.59 kW	1.32 kW	2.9 kW	13.49%	68.86%
HC-TCT	6.57 kW	1.34 kW	3 kW	13.45%	68.65%
BL-HC	6.51 kW	1.4 kW	3.06 kW	13.33%	68.02%
Static Recon-figuration	6.90 kW	1.01 kW	2.67 kW	14.12%	72.10%
Two-Step Approach	7.78 kW	0.13 kW	1.79 kW	15.93%	81.29%
Partial Shading S3					
Configuration	Power Output	ML	PR	E	P Index
SP	7.50 kW	1.38 kW	2.47 kW	14.53%	74.19%
BL	7.52 kW	0.96 kW	2.05 kW	15.39%	78.57%
HC	7.55 kW	0.93 kW	2.02 kW	15.46%	78.89%
TCT	7.73 kW	0.75 kW	1.84 kW	15.82%	80.77%
SP-TCT	7.70 kW	0.78 kW	1.87 kW	15.76%	80.45%
BL-TCT	7.70 kW	0.78 kW	1.87 kW	15.76%	80.45%
HC-TCT	7.72 kW	0.76 kW	1.85 kW	15.80%	80.66%
BL-HC	7.59 kW	0.89 kW	1.98 kW	15.54%	79.31%
Static Recon-figuration	8.30 kW	0.18 kW	1.27 kW	16.99%	86.72%
Two-Step Approach	8.48 kW	0.06 kW	1.15 kW	17.24%	87.98%
Partial Shading S4					
Configuration	Power Output	ML	PR	E	P Index
SP	7.88 kW	0.89 kW	1.69 kW	16.13%	82.34%
BL	8 kW	0.77 kW	1.57 kW	16.38%	83.59%
HC	8.12 kW	0.65 kW	1.45 kW	16.62%	84.84%
TCT	8.50 kW	0.27 kW	1.07 kW	17.40%	88.81%
SP-TCT	8.13 kW	0.64 kW	1.44 kW	16.64%	84.95%
BL-TCT	8.06 kW	0.71 kW	1.51 kW	16.50%	84.22%
HC-TCT	8.15 kW	0.62 kW	1.42 kW	16.68%	85.16%
BL-HC	8.10 kW	0.67 kW	1.47 kW	16.58%	84.63%
Static Recon-figuration	8.21 kW	0.56 kW	1.36 kW	16.81%	85.78%
Two-Step Approach	8.85 kW	0 kW	0.62 kW	18.32%	93.52%



**Table 4.** *Cont.*

Configuration	Partial Shading S5				
	Power Output	ML	PR	E	P Index
SP	4.42 kW	4.44 kW	5.15 kW	9.05%	46.18%
BL	3.7 kW	5.16 kW	5.87 kW	7.57%	38.66%
HC	3.87 kW	4.99 kW	5.7 kW	7.92%	40.43%
TCT	5.71 kW	3.15 kW	3.86 kW	11.69%	59.66%
SP-TCT	4.78 kW	4.08 kW	4.79 kW	9.78%	49.94%
BL-TCT	4.78 kW	4.08 kW	4.79 kW	9.78%	49.94%
HC-TCT	4.77 kW	4.09 kW	4.8 kW	9.76%	49.84%
BL-HC	4.78 kW	4.09 kW	4.8 kW	9.76%	49.84%
Static Reconfiguration	4.02 kW	4.84 kW	5.55 kW	8.23%	42%
Two-Step Approach	5.85 kW	3.01 kW	3.72 kW	11.97%	61.12%

**Table 5.** Power output of PV array configurations for random shading cases.

Shading Case	SP	BL	HC	TCT	SP-TCT	BL-TCT	HC-TCT	BL-HC	SER	Two-Step Approach
I	6.17	6.31	6.24	6.47	6.36	6.33	6.38	6.31	6.92	7.87
II	6.92	7.11	7.14	7.36	7.27	7.24	7.28	7.22	7.31	7.88
III	8.00	8.10	8.10	8.19	8.06	8.07	8.10	8.10	8.20	8.70
IV	7.99	8.27	8.24	8.14	8.28	8.26	8.26	8.27	8.21	8.91
V	5.27	5.53	5.87	7.11	7.06	7.05	7.06	6.45	7.21	7.76
VI	4.72	4.69	4.72	4.70	4.70	4.70	4.69	4.69	4.79	5.96
VII	7.39	7.59	7.95	8.32	8.30	8.31	8.30	8.24	8.41	8.95
VIII	4.71	4.57	4.62	4.57	4.58	4.57	4.58	4.58	4.76	5.93
IX	9.12	9.12	9.12	9.14	9.13	9.12	9.13	9.13	9.14	9.54
X	3.48	3.48	3.48	3.48	3.48	3.48	3.48	3.48	3.68	4.89

All values in the table are kW units. SER—Static Electrical Reconfiguration.

### 5.2. Asymmetric $18 \times 3$ PV Array

The application of the proposed two-step approach was validated using the  $16 \times 3$  (long) array, which was placed in the  $8 \times 6$  architecture in an irradiance block, i.e., the first two columns contain a single string of 16 modules, with eight modules in a column. Similarly, columns 2 and 3 contain another string with eight modules in a single column, and so on. The array was evaluated by considering the partial shading condition that starts from the top of the array, moves towards the bottom, and ends with different irradiance levels, as shown in Figure 18. The array operates under the no shading condition in case A, whereas shading develops in case B, with the first row receiving  $600 \text{ W/m}^2$ , before progressively moving downward for case C, with irradiance levels of  $600 \text{ W/m}^2$  and  $550 \text{ W/m}^2$ . The partial shading progressively moves in a downward direction until case Q, where the partial shading ends. The P~V curves of the respective partial shading cases are shown in Figure 19, where it can be observed that under these types of shading conditions, all the configurations under comparison have equal power output, with the two-step approach generating higher power for all cases. The power output by configuration for case A, case B, case C, case D, case E, case F, case G, case H, case I, case J, case K, case L, case M, case N, case O, case P and case Q were determined to be 13.41 kW, 11.68 kW, 10.14 kW, 9.24 kW, 8.36 kW, 7.45 kW, 6.53 kW, 5.65 kW, 4.86 kW, 4.86 kW, 4.89 kW, 4.91 kW, 6.49 kW, 8.22 kW, 9.95 kW, 11.68 kW and 13.41 kW, respectively, whereas when using the two-step

approach, the power output was established to be 13.41 kW, 12.72 kW, 12.31 kW, 11.22 kW, 10.61 kW, 9.13 kW, 8.24 kW, 7.30 kW, 6.39 kW, 6.42 kW, 6.48 kW, 7.30 kW, 7.83 kW, 8.49 kW, 10.69 kW, 11.99 kW and 13.41 kW, respectively. The comparison of the power output for all the configurations and the two-step approach is graphically represented in Figure 20, from which it can be observed that for an increasing level of partial shading from case A to I, and subsequently decreasing shading from case I to Q, the two-step approach generated the highest power output. Additionally, the comparison of the efficiency and performance index for all partial shading cases is shown in Figure 21, from which it can be observed that the two-step approach presents higher values than the others.

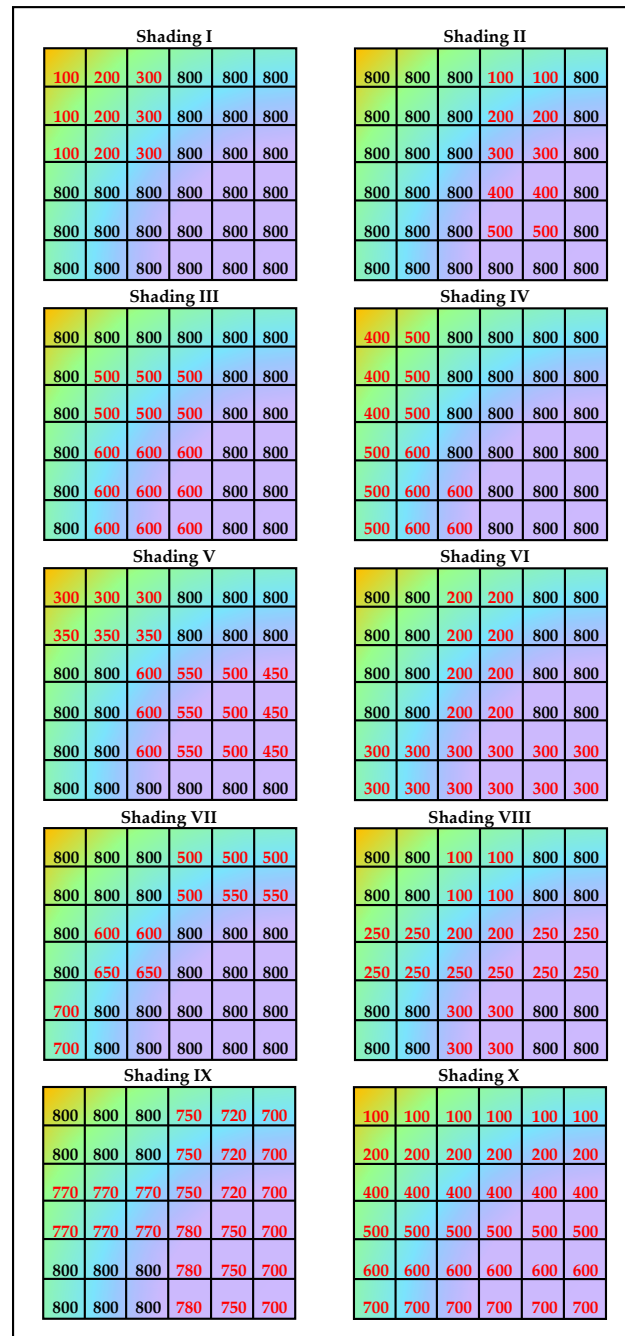


Figure 16. Random partial shading cases for the 6 × 6 PV array.

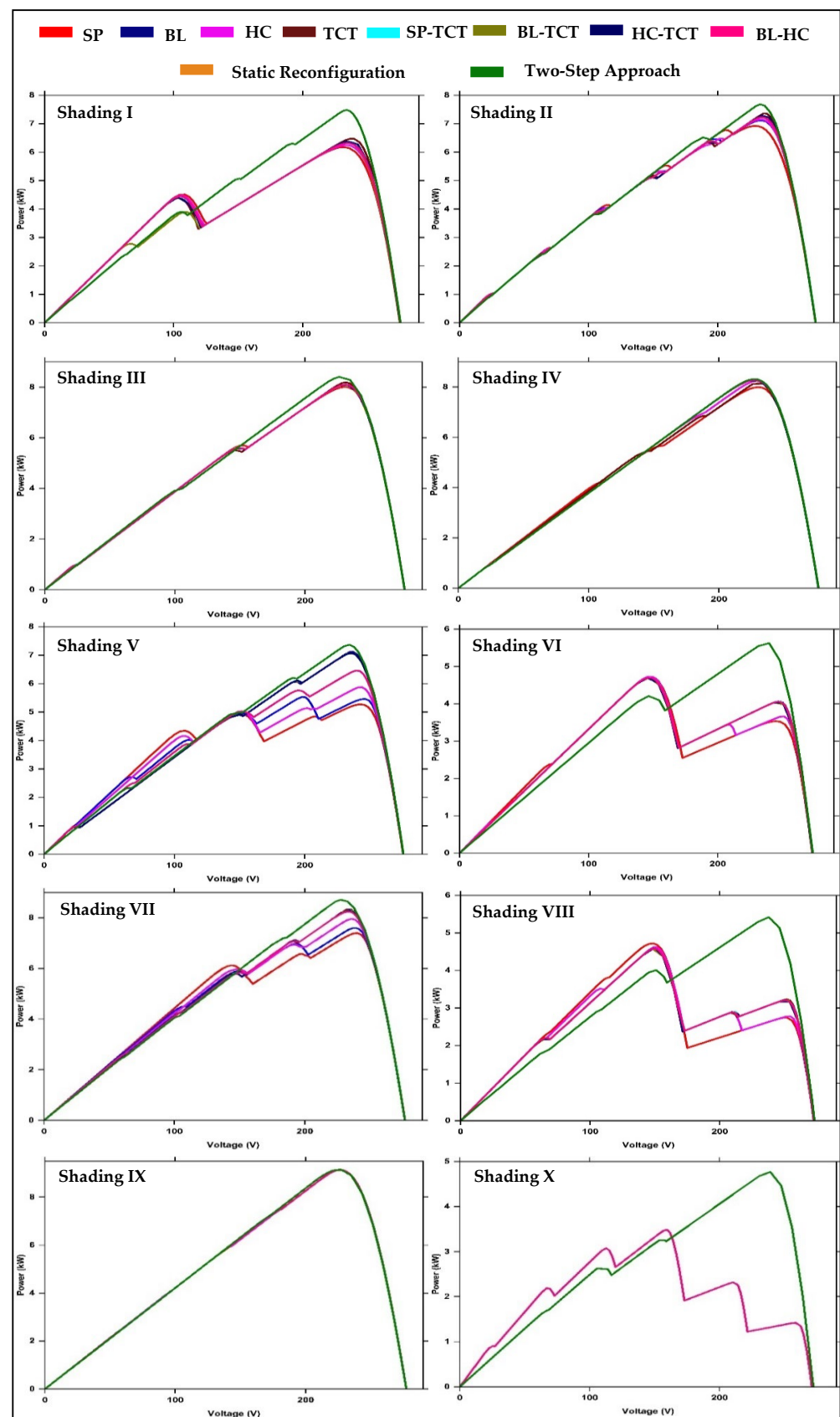
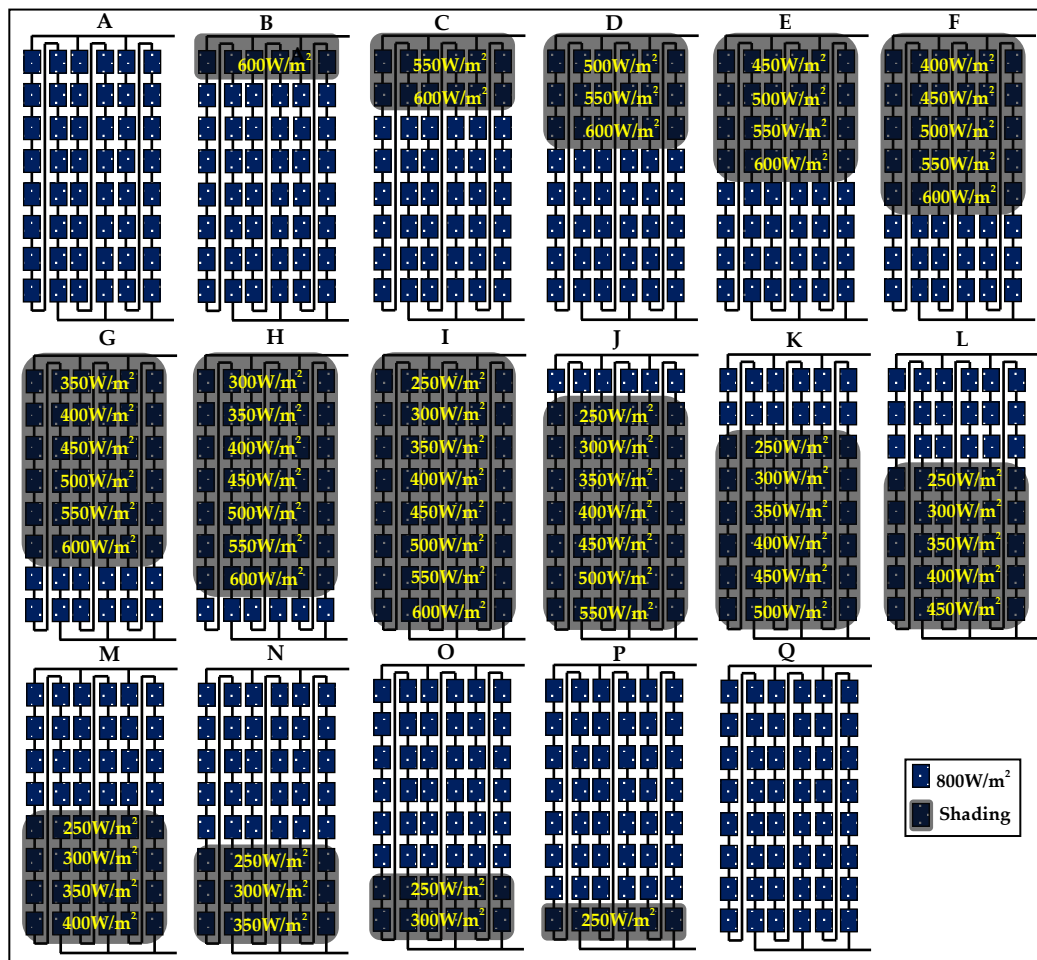


Figure 17. P~V curves of the array configurations under different random partial shading cases.



**Figure 18.** Partial shading cases for  $18 \times 3$  PV arrays with different configurations, static reconfiguration, and the two-step approach.

Hence, the analysis conducted in this paper shows the efficacy of the proposed technique compared to conventional and hybrid configurations and static reconfiguration under a variety of partial shading cases. Additionally, the two-step approach overcomes the limitations of different configurations with regard to symmetric application by exhibiting wide applicability for arbitrary array sizes. For the  $6 \times 6$  array, the average power enhancements of the two-step approach compared to the SP, BL, HC, TCT, SP-TCT, BL-TCT, HC-TCT, BL-HC and static electrical reconfiguration were noted to be 15.35%, 20.15%, 18.21%, 6.46%, 11.74%, 11.90%, 11.73%, 12.44% and 14.60%, respectively. Similarly, for random partial shading cases for a  $6 \times 6$  array, the average power enhancement of the two-step approach was calculated to be 22.73%, 21.09%, 19.65%, 16.25%, 16.67%, 16.68%, 16.61%, 17.94% and 13.64% compared to SP, BL, HC, TCT, SP-TCT, BL-TCT, HC-TCT, BL-HC and static reconfiguration, respectively. Similarly, for the  $16 \times 3$  array, the two-step approach had an average power 22.41% higher than that of other configurations during partial shading. Therefore, on the basis of these results, it can be stated that the two-step approach has a higher power output and performance under all partial shading conditions.

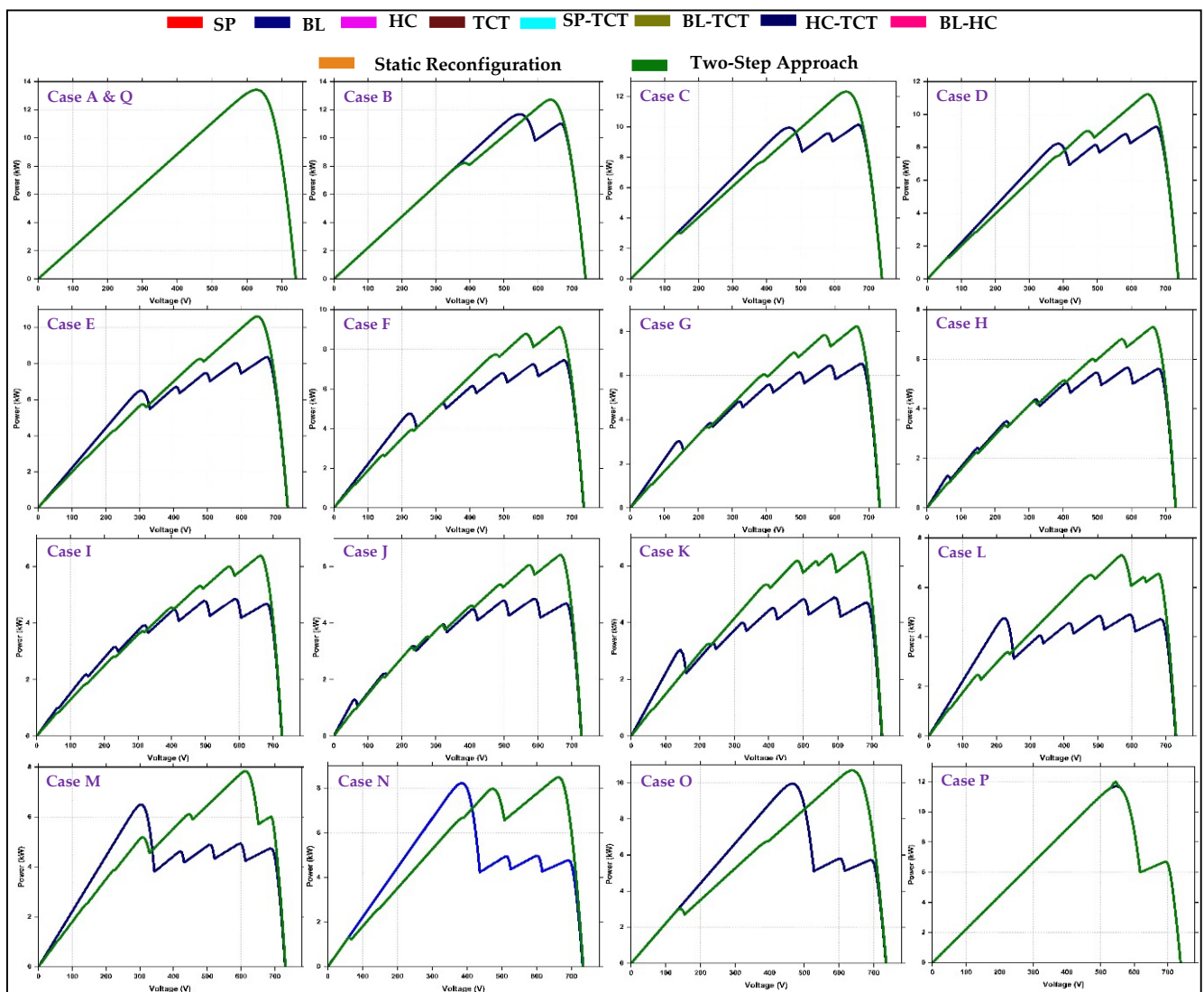


Figure 19. P~V curves for the partial shading cases in an  $18 \times 3$  PV array with conventional and hybrid configurations using the two-step approach.

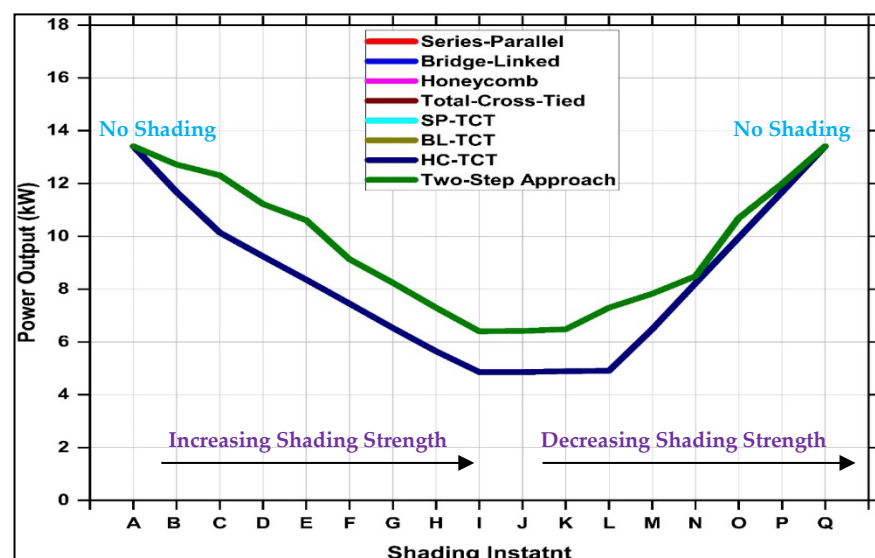
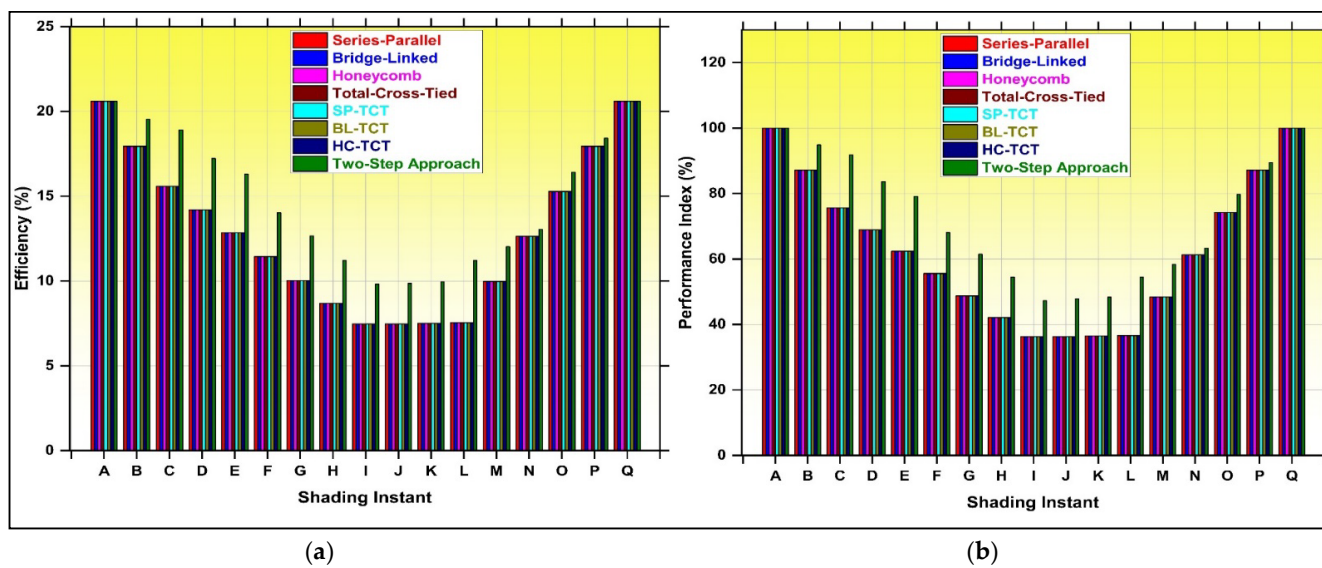


Figure 20. Power output comparison of  $18 \times 3$  array for partial shading cases.





**Figure 21.** Comparison of (a) efficiency and (b) performance index of the  $8 \times 3$  configurations using the proposed two-step approach for partial shading cases.

## 6. Conclusions

A two-step approach for module placement with the aim of increasing the power output of the PV arrays during partial shading was proposed in this paper. The approach was validated under numerous partial shading cases and its performance compared with that of conventional configurations such as SP, BL, HC and TCT, hybrid configurations such as SP-TCT, BL-TCT, HC-TCT and BL-HC, and a static electrical reconfiguration technique. The application of the two-step approach in symmetrical and asymmetrical array sizes was verified for two array sizes— $6 \times 6$  (short) and  $16 \times 3$  (long)—under numerous partial shading cases. On the basis of the analysis conducted in this paper, the following conclusions regarding the advantages of the proposed two-step approach were drawn:

- Output value 5.35%, 20.15%, 18.21%, 6.46%, 11.74%, 11.90%, 11.73%, 12.44% and 14.60% higher than in the SP, BL, HC, TCT, SP-TCT, BL-TCT, HC-TCT, BL-HC and static reconfiguration in the  $6 \times 6$  array.
- Power output 22.73%, 21.09%, 19.65%, 16.25%, 16.67%, 16.68%, 16.61%, 17.94% and 13.64% higher than in the SP, BL, HC, TCT, SP-TCT, BL-TCT, HC-TCT, BL-HC and static reconfiguration in the  $6 \times 6$  array under random shading.
- Power output 22.14% higher than in all other configurations in the  $16 \times 3$  array.
- Reduced losses, higher performance and higher efficiency compared to other configurations in all partial shading cases.
- Applicable for both symmetric and asymmetric arrays.
- Requires no switches, sensors, or complex algorithms.
- Wide practical application.
- Easy to implement in PV arrays.

Hence, it can be stated that implementation of the proposed two-step approach in PV arrays can increase their reliability and reduce the chances of system failure under partial shading conditions.

**Author Contributions:** All authors have contributed equally to the idea and the design of the methodology proposed and to the deployment of the research paper. Conceptualization, P.R.S.; methodology, P.R.S.; software, P.R.S. and S.R.K.M.; validation, P.R.S., B.A. and S.B.T.; formal analysis, P.R.S. and P.V.; investigation, P.R.S. and S.B.T.; resources, B.A. and S.B.T.; writing—original draft preparation, P.R.S.; writing—review and editing, P.R.S. and P.V.; visualization, P.R.S. and S.R.K.M.; supervision, S.B.T.; project administration, B.A. and S.B.T. All authors have read and agreed to the published version of the manuscript.

**Funding:** The authors are thankful to the Deanship of Scientific Research at Najran University for funding this work under the Research Groups funding program grant code (NU/RG/SERC/11/6).

**Data Availability Statement:** Not applicable.

**Conflicts of Interest:** The authors declare no conflict of interest.

## References

1. Al-Badi, A.; Al Wahaibi, A.; Ahshan, R.; Malik, A. Techno-Economic Feasibility of a Solar-Wind-Fuel Cell Energy System in Duqm, Oman. *Energies* **2022**, *15*, 5379. [\[CrossRef\]](#)
2. Goh, H.H.; Li, C.; Zhang, D.; Dai, W.; Lim, C.S.; Kurniawan, T.A.; Goh, K.C. Application of choosing by advantages to determine the optimal site for solar power plants. *Sci. Rep.* **2022**, *12*, 4113. [\[CrossRef\]](#) [\[PubMed\]](#)
3. Kılıç, U.; Kekezoğlu, B. A review of solar photovoltaic incentives and Policy: Selected countries and Turkey. *Ain Shams Eng. J.* **2022**, *13*, 101669. [\[CrossRef\]](#)
4. Raza, F.; Tamoor, M.; Miran, S.; Arif, W.; Kiren, T.; Amjad, W.; Lee, G.H. The socio-economic impact of using Photovoltaic (PV) energy for high-efficiency irrigation systems: A case study. *Energies* **2022**, *15*, 1198. [\[CrossRef\]](#)
5. Kuo, T.C.; Pham, T.T.; Huang, P.T.; Nguyen, H.T.; Bui, D.M.; Le, P.D. Reliability analysis of PV generating systems in the islanded DC microgrid under dynamic and transient operation. *IET Renew. Power Gener.* **2022**, *16*, 988–1026. [\[CrossRef\]](#)
6. Rezazadeh, S.; Moradzadeh, A.; Pourhossein, K.; Akrami, M.; Mohammadi-Ivatloo, B.; Anvari-Moghaddam, A. Photovoltaic array reconfiguration under partial shading conditions for maximum power extraction: A state-of-the-art review and new solution method. *Energy Convers. Manag.* **2022**, *258*, 115468. [\[CrossRef\]](#)
7. Osmani, K.; Haddad, A.; Jaber, H.; Lemenand, T.; Castanier, B.; Ramadan, M. Mitigating the effects of partial shading on PV system's performance through PV array reconfiguration: A review. *Therm. Sci. Eng. Prog.* **2022**, *31*, 101280. [\[CrossRef\]](#)
8. Wolf, E.J.; Gould, I.E.; Bliss, L.B.; Berry, J.J.; McGehee, M.D. Designing modules to prevent reverse bias degradation in perovskite solar cells when partial shading occurs. *Sol. RRL* **2022**, *6*, 2100239. [\[CrossRef\]](#)
9. Wasim, M.S.; Amjad, M.; Habib, S.; Abbasi, M.A.; Bhatti, A.R.; Mueen, S.M. A critical review and performance comparisons of swarm-based optimization algorithms in maximum power point tracking of photovoltaic systems under partial shading conditions. *Energy Rep.* **2022**, *8*, 4871–4898. [\[CrossRef\]](#)
10. Rehman, H.; Murtaza, A.F.; Sher, H.A.; Noman, A.M.; Al-Shamma'a, A.A.; Alkuhayli, A.; Spertino, F. Neighboring-Pixel-Based maximum power point tracking algorithm for partially shaded photovoltaic (PV) systems. *Electronics* **2022**, *11*, 359. [\[CrossRef\]](#)
11. Ye, S.P.; Liu, Y.H.; Wang, S.C.; Pai, H.Y. A novel global maximum power point tracking algorithm based on Nelder-Mead simplex technique for complex partial shading conditions. *Appl. Energy* **2022**, *321*, 119380.
12. Chtita, S.; Motahhir, S.; El Hammoumi, A.; Chouder, A.; Benyoucef, A.S.; El Ghzizal, A.; Askar, S.S. A novel hybrid GWO-PSO-based maximum power point tracking for photovoltaic systems operating under partial shading conditions. *Sci. Rep.* **2022**, *12*, 10637. [\[CrossRef\]](#) [\[PubMed\]](#)
13. Vadivel, S.; Sengodan, B.C.; Ramasamy, S.; Ahsan, M.; Haider, J.; Rodrigues, E.M. Social Grouping Algorithm Aided Maximum Power Point Tracking Scheme for Partial Shaded Photovoltaic Array. *Energies* **2022**, *15*, 2105. [\[CrossRef\]](#)
14. Akram, N.; Khan, L.; Agha, S.; Hafeez, K. Global Maximum Power Point Tracking of Partially Shaded PV System Using Advanced Optimization Techniques. *Energies* **2022**, *15*, 4055. [\[CrossRef\]](#)
15. Shams, I.; Mekhilef, S.; Tey, K.S. Advancement of voltage equalizer topologies for serially connected solar modules as partial shading mitigation technique: A comprehensive review. *J. Clean. Prod.* **2021**, *285*, 124824. [\[CrossRef\]](#)
16. Satpathy, P.R.; Babu, T.S.; Mahmoud, A.H.; Sharma, R.; Nastasi, B. A TCT-SC hybridized voltage equalizer for partial shading mitigation in PV arrays. *IEEE Trans. Sustain. Energy* **2021**, *12*, 2268–2281. [\[CrossRef\]](#)
17. Uno, M.; Suzuki, T.; Fujii, Y. Module-to-Panel Modular Differential Power Processing Converter with Isolated DC Bus for Photovoltaic Systems Under Partial Shading. *IEEE J. Emerg. Sel. Top. Ind. Electron.* **2022**, *1*–11. [\[CrossRef\]](#)
18. Uno, M.; Sato, H.; Oyama, S. Switched Capacitor-Based Modular Differential Power Processing Architecture for Large-Scale Photovoltaic Systems Under Partial Shading. *IEEE Trans. Energy Convers.* **2022**, *37*, 1545–1556. [\[CrossRef\]](#)
19. Satpathy, P.R.; Jena, S.; Sharma, R. Power enhancement from partially shaded modules of solar PV arrays through various interconnections among modules. *Energy* **2018**, *144*, 839–850. [\[CrossRef\]](#)
20. Pachauri, R.K.; Mahela, O.P.; Sharma, A.; Bai, J.; Chauhan, Y.K.; Khan, B.; Alhelou, H.H. Impact of partial shading on various PV array configurations and different modeling approaches: A comprehensive review. *IEEE Access* **2020**, *8*, 181375–181403. [\[CrossRef\]](#)
21. Lappalainen, K.; Valkealahti, S. Output power variation of different PV array configurations during irradiance transitions caused by moving clouds. *Appl. Energy* **2017**, *190*, 902–910. [\[CrossRef\]](#)
22. Satpathy, P.R.; Babu, T.S.; Shanmugam, S.K.; Popavath, L.N.; Alhelou, H.H. Impact of uneven shading by neighboring buildings and clouds on the conventional and hybrid configurations of roof-top PV arrays. *IEEE Access* **2021**, *9*, 139059–139073. [\[CrossRef\]](#)
23. Krishna, G.S.; Moger, T. Reconfiguration strategies for reducing partial shading effects in photovoltaic arrays: State of the art. *Sol. Energy* **2019**, *182*, 429–452. [\[CrossRef\]](#)
24. La Manna, D.; Vigni, V.L.; Sanseverino, E.R.; Di Dio, V.; Romano, P. Reconfigurable electrical interconnection strategies for photovoltaic arrays: A review. *Renew. Sustain. Energy Rev.* **2014**, *33*, 412–426. [\[CrossRef\]](#)

25. Aljafari, B.; Satpathy, P.R.; Thanikanti, S.B. Partial shading mitigation in PV arrays through dragonfly algorithm based dynamic reconfiguration. *Energy* **2022**, *257*, 124795. [[CrossRef](#)]
26. Solis-Cisneros, H.I.; Sevilla-Camacho, P.Y.; Robles-Ocampo, J.B.; Zuñiga-Reyes, M.A.; Rodríguez-Resendíz, J.; Muñoz-Soria, J.; Hernández-Gutiérrez, C.A. A dynamic reconfiguration method based on neuro-fuzzy control algorithm for partially shaded PV arrays. *Sustain. Energy Technol. Assess.* **2022**, *52*, 102147. [[CrossRef](#)]
27. Alanazi, M.; Fathy, A.; Yousri, D.; Rezk, H. Optimal reconfiguration of shaded PV based system using African vultures optimization approach. *Alex. Eng. J.* **2022**, *61*, 12159–12185. [[CrossRef](#)]
28. Gao, X.; Deng, F.; Zheng, H.; Ding, N.; Ye, Z.; Cai, Y.; Wang, X. Followed The Regularized Leader (FTRL) prediction model based photovoltaic array reconfiguration for mitigation of mismatch losses in partial shading condition. *IET Renew. Power Gener.* **2022**, *16*, 159–176. [[CrossRef](#)]
29. Durango-Flórez, M.; González-Montoya, D.; Trejos-Grisales, L.A.; Ramos-Paja, C.A. PV Array Reconfiguration Based on Genetic Algorithm for Maximum Power Extraction and Energy Impact Analysis. *Sustainability* **2022**, *14*, 3764. [[CrossRef](#)]
30. Rao, P.S.; Ilango, G.S.; Nagamani, C. Maximum power from PV arrays using a fixed configuration under different shading conditions. *IEEE J. Photovolt.* **2014**, *4*, 679–686.
31. Rani, B.I.; Ilango, G.S.; Nagamani, C. Enhanced power generation from PV array under partial shading conditions by shade dispersion using Su Do Ku configuration. *IEEE Trans. Sustain. Energy* **2013**, *4*, 594–601. [[CrossRef](#)]
32. Vijayalekshmy, S.; Bindu, G.R.; Iyer, S.R. A novel Zig-Zag scheme for power enhancement of partially shaded solar arrays. *Sol. Energy* **2016**, *135*, 92–102. [[CrossRef](#)]
33. Harish Kumar Varma, G.; Barry, V.R.; Jain, R.K. A novel magic square based physical reconfiguration for power enhancement in larger size photovoltaic array. *IETE J. Res.* **2021**, 1–14. [[CrossRef](#)]
34. Reddy, S.S.; Yammani, C. A novel Magic-Square puzzle based one-time PV reconfiguration technique to mitigate mismatch power loss under various partial shading conditions. *Optik* **2020**, *222*, 165289. [[CrossRef](#)]
35. Yousri, D.; Fathy, A.; El-Saadany, E.F. Four square sudoku approach for alleviating shading effect on total-cross-tied PV array. *Energy Convers. Manag.* **2022**, *269*, 116105. [[CrossRef](#)]
36. Pachauri, R.K.; Thanikanti, S.B.; Bai, J.; Yadav, V.K.; Aljafari, B.; Ghosh, S.; Alhelou, H.H. Ancient Chinese magic square-based PV array reconfiguration methodology to reduce power loss under partial shading conditions. *Energy Convers. Manag.* **2022**, *253*, 115148. [[CrossRef](#)]
37. Yang, Z.; Zhang, N.; Wang, J.; Liu, Y.; Fu, L. Improved non-symmetrical puzzle reconfiguration scheme for power loss reduction in photovoltaic systems under partial shading conditions. *Sustain. Energy Technol. Assess.* **2022**, *51*, 101934. [[CrossRef](#)]
38. Nihanth MS, S.; Ram, J.P.; Pillai, D.S.; Ghias, A.M.; Garg, A.; Rajasekar, N. Enhanced power production in PV arrays using a new skyscraper puzzle based one-time reconfiguration procedure under partial shade conditions (PSCs). *Sol. Energy* **2022**, *194*, 209–224. [[CrossRef](#)]
39. Palpandian, M.; Winston, D.P.; Kumar, B.P.; Kumar, C.S.; Babu, T.S.; Alhelou, H.H. A new ken-ken puzzle pattern based reconfiguration technique for maximum power extraction in partial shaded solar PV array. *IEEE Access* **2021**, *9*, 65824–65837. [[CrossRef](#)]
40. Satpathy, P.R.; Bhowmik, P.; Babu, T.S.; Sain, C.; Sharma, R.; Alhelou, H.H. Performance and Reliability Improvement of Partially Shaded PV Arrays by One-Time Electrical Reconfiguration. *IEEE Access* **2022**, *10*, 46911–46935. [[CrossRef](#)]
41. Raj RD, A.; Naik, K.A. Optimal reconfiguration of PV array based on digital image encryption algorithm: A comprehensive simulation and experimental investigation. *Energy Convers. Manag.* **2022**, *261*, 115666. [[CrossRef](#)]
42. Yang, B.; Ye, H.; Wang, J.; Li, J.; Wu, S.; Li, Y.; Ye, H. PV arrays reconfiguration for partial shading mitigation: Recent advances, challenges and perspectives. *Energy Convers. Manag.* **2021**, *247*, 114738. [[CrossRef](#)]